Efficient analysis of 2D antenna arrays using the ASM-MBF method

SERGIO AMAYA MALDONADO

KTH Electrical Engineering

Masters' Degree Project
Stockholm, Sweden June 2011

XR-EE-ETK 2011:006

KTH Electrical Engineering

Efficient analysis of 2D antenna arrays using the ASM-MBF method

Departament of Electromagnetic Theory

SERGIO AMAYA MALDONADO

Master Thesis at KTH
Supervisor: Anders Ellgardt
Examiner: Lars Jonsson

XR-EE-ETK 2011:006

Abstract

The analysis of large-scaled 2D finite planar arrays with the Method of Moments relying on the RWG basis functions requires a huge amount of memory for saving the equation system and a long computation time for solving the surface current distribution. In this project, the Array Scanning Method - Macro Basis Function (ASM-MBF) method created by Craeye is implemented in an existing MoM's code in order to verify the reduction of the equation system keeping a good accuracy. Some improvements have been implemented in the existing code in order to analyze arrays with rectangular and skew lattices. The time spent in the impedance matrix construction has also been reduced. A program for solving 2D infinite arrays has been created for obtaining the infinite surface current distributions necessary for the implementation of the ASM-MBF method. Finally, the definitive program has been tested with arrays of dipole and bowtie antennas. In both cases, the computation time is reduced without affecting the accuracy of the input impedance.

Contents

List of Figures

List of Acronyms

EFIE	Electric Field Integral Equation
MFIE	Magnetic Field Integral Equation
MoM	Method of Moments
RWG	Rao-Wilton-Glison
MBF	Macro Basis Functions
CBF	Characteristic Basis Functions
PEC	Perfectly Electrical Conductor
ASM	Array Scanning Method
ASM-MBF	Array Scanning Method - Macro Basis Functions
PMCHWT	Poggio-Miller-Chang-Harrington-Wu-Tsai
SVD	Single Value Decomposition
NEC-2	Numerical Electromagnetic Code
FDTD	Finite-Difference Time-Domain
PGF	Periodic Green's Function

Chapter 1

Introduction

The electromagnetic analysis of large-scaled periodic structures is usually time-consuming, especially for 2D-planar arrays of antennas. For arbitrary antennas, the Electric Field Integral Equation (EFIE) and the Magnetic Field Integral Equation (MFIE) [1] formulations are utilized. The EFIE can be applied to open and closed antenna surfaces, but not in wires. However, this type of geometry is approximated with thin strips [2-3]. The MFIE is only useful for open bodies.

The Method of Moments (MoM) technique [4] is typically applied to the EFIE for solving the surface current distribution. The basic problem consists of finding the current as a linear combination of a set of known basis functions such as the Rao-Wilton-Glison (RWG) functions [5]. This RWG procedure discretizes the surface of the antennas forming the analyzed structure into a triangular grid. Every inner edge of the mesh is defined as a function weighted by an unknown coefficient. Depending on the refinement of the mesh and the dimensions of the array, the number of unknowns can be extremely large. This implies that the impedance matrix containing the mutual coupling effects between edges of the resultant system of equations can be huge. Thus, solving the system will require a long computation time.

Fortunately, in the past recent years, several novel methods have arisen improving the array analysis in terms of computation efficiency. Some of them are related to the infinite-array approximation [6-8]. In these techniques, the problem is approached solving the infinite case adding some corrections for the array edge effects. This method is particularly useful when one is working with large periodic finite structures because the inner currents have the same behavior in both cases. Other approximations involve the idea of defining a set of global surface current distributions obtained from the solution of simple problems for replacing the formerly subdomain functions. The number of these high-level functions is lower than the number of subdomain functions. This means that applying these new functions the system of equations and the number of unknowns are reduced considerably. These distributions are called Macro Basis functions (MBF) or Characteristic Basis Functions (CBF) [9-10] in which primary and secondary functions, extracted from the primary ones, are obtained in order to represent accurately the mutual coupling effects.

The Array Scanning Method - Macro Basis Function (ASM-MBF) Method [11] combines the fundamental concepts of the infinite and finite approximations. This technique is based on obtaining a set of high-level functions for reducing the dimensions of the equation system. This set of MBFs is extracted from the infinite array solution using the Array Scanning Method (ASM) for the inner currents and from the full-wave solution of a 2×2 array for the edge effects. The computation cost for solving the reduced system is negligible with

respect to the original one, providing an excellent accuracy.

The present project has been implemented in the Method of Moment's code developed by Makarov [12]. It is based on the EFIE formulation and the RWG subdomain functions. This code is focused on solving arbitrary antenna geometries made of perfectly electrical conductor (PEC). The main parts of the thesis are:

- Verification of the MoM's code accuracy.
- Modification of the code for building 2D planar array meshes with rectangular and skew lattices from a basic antenna mesh.
- Improvement of the efficiency of the impedance matrix construction. The accuracy of the input impedance was also evaluated.
- Implementation of the 3D periodic Green's function so as to solve 2D infinite arrays. In addition, a method for improving the convergence of the function was tested and applied.
- Extraction of the MBFs from the infinite arrays code using the ASM and from the original code.
- Implementation of the ASM-MBF method and evaluation of the computation time and the accuracy of the input impedance.

Chapter 2

Background theory

In this section, the basic theory about the motivation of the project and the improvements that have been implemented is discussed. The EFIE formulation is first recalled for a general electromagnetic problem. This formulation is exemplified for finite and infinite arrays. The periodic Green's function needed in the infinite array formulation has a very slowly convergent series to determine its value. For that reason, some techniques for accelerating the convergence of the expression are discussed. The expressions are especially focused on antenna arrays in 3D space with 2D periodicity, which is the main case considered in this project. The basic concepts of the MoM are commented taking the EFIE equation as the starting point. The discretization of the antenna surface and the application of RWG basis functions to the MoM are also explained. Finally, the MBF concept is introduced with special emphasis in the ASM-MBF method, which is used to reduce the computation time.

Note that this work is limited to perfectly electrical conductor (PEC) objects due to the use of EFIE formulation. For the hypothetical case of working with dielectric materials, the PMCHWT (Poggio-Miller-Chang-Harrington-Wu-Tsai) formulation [13] and Levin T accelerator [14] should be used instead.

2.1 EFIE formulation

A general problem involving an antenna made of PEC working in transmission mode is considered below following the formulation presented in [4]. From a known port excitation the goal is to resolve the surface current distribution.The electrical field radiated by the antenna surface is given by the following expression:

$$\mathbf{E}^s = -j\omega\mathbf{A} - \frac{j}{\omega\mu\epsilon}\nabla\left(\nabla\cdot\mathbf{A}\right) \tag{2.1}$$

where ω is the angular frequency, μ and ϵ are the permeability and the permittivity of the medium, and $\mathbf{A}$ is the magnetic vector potential, expressed as:

$$\mathbf{A}(\mathbf{r}) = \mu \iint_S G(\mathbf{r},\mathbf{r}')\mathbf{J}(\mathbf{r}')\mathrm{d}\mathbf{r}' \tag{2.2}$$

Here S is the scattering surface of the antenna, $\mathbf{J}(\mathbf{r}')$ is the surface current distribution, $\mathbf{r}$ and $\mathbf{r}'$ the observation point and the integration point respectively, and

$$G(\mathbf{r},\mathbf{r}') = \frac{1}{4\pi}\frac{e^{-jk|\mathbf{r}-\mathbf{r}'|}}{|\ \mathbf{r}-\mathbf{r}'\ |} \tag{2.3}$$

is the free Helmholtz 3-dimensional Green's function. To solve equation in (2.1) for $\mathbf{J}(\mathbf{r}')$ a boundary condition is needed due to the unknown scattered electric field $\mathbf{E}^s$. The tangential electric field of the antenna surface satisfies:

$$-\widehat{\mathbf{n}}(\mathbf{r}) \times \mathbf{E}^i(\mathbf{r}) = \widehat{\mathbf{n}}(\mathbf{r}) \times \mathbf{E}^s(\mathbf{r}) \tag{2.4}$$

In this equation, $\widehat{\mathbf{n}}(\mathbf{r})$ is the unitary vector normal to the antenna surface and $\mathbf{E}^i(\mathbf{r})$ is the incident electric field exciting the antenna. In this case, we consider only the radiation problem. The feeding points are approximated as voltage gaps of infinitesimal width. This excitation is expressed as a Dirac delta, $\delta(d)$ of an amplitude V:

$$\mathbf{E}^i(\mathbf{r}) = -\nabla\varphi = \frac{V}{\Delta} \cong V\delta(d) \tag{2.5}$$

where d is the variable representing the infinitesimal width of the gap, φ is the electric potential and Δ is the gap of negligible width. Thus, replacing $\mathbf{E}^i(\mathbf{r})$ and $\mathbf{E}^s(\mathbf{r})$ in (2.4) for the equations in (2.5) and (2.1) respectively:

$$-\frac{j}{\omega}\widehat{\mathbf{n}}(\mathbf{r}) \times V\delta(d) = \widehat{\mathbf{n}}(\mathbf{r}) \times \left[\mathbf{A}(\mathbf{r}) + \frac{1}{k^2}\nabla\nabla \cdot \mathbf{A}(\mathbf{r})\right] \tag{2.6}$$

where k is the wavenumber. The equation in (2.6) is the EFIE particularized for the case analyzed in this section. The current $\mathbf{J}(\mathbf{r}')$ is obtained directly from this expression using (2.2).

2.2 Finite arrays

An array is defined as a set of antennas uniformly spaced that are fed coherently. Every feeding port is controlled in phase and distance for beamforming purposes. An antenna does not have the same behavior when it is isolated or is inside an array structure. The reason is that every antenna is affected by the mutual coupling of the surrounding cells.

The EFIE in (2.6) is now extrapolated to this array interaction problem. It is considered the analysis of the mutual coupling of an array of arbitrary shaped antennas. Supposing that the array has N elements, the integrodifferential equation for the n^{th} port will be:

$$-\frac{j}{\omega}\widehat{\mathbf{n}}(\mathbf{r}_n) \times V_n\delta(w) = \widehat{\mathbf{n}}(\mathbf{r}_n) \times \left(1 + \frac{1}{k^2}\nabla\nabla\right)\left[\sum_m \mathbf{A}^m(\mathbf{r}_n)\right] \; 1 \leq n \leq N \tag{2.7}$$

where $\mathbf{A}^m(\mathbf{r}_n)$ is the magnetic potential vector for m^{th} antenna which can also be expressed as:

$$\begin{aligned} -\frac{j}{\omega}\widehat{\mathbf{n}}(\mathbf{r}_n) \times V_n\delta(w) &= \widehat{\mathbf{n}}(\mathbf{r}_n)\times \\ &\times \left(1 + \frac{1}{k^2}\nabla\nabla\right)\left[\mu\sum_m \iint_S G(\mathbf{r}_n, \mathbf{r}'_m)\mathbf{J}_m(\mathbf{r}'_m)\mathrm{d}\mathbf{r}'_m\right] \; 1 \leq n \leq N \end{aligned} \tag{2.8}$$

Here the subindex n defines the antenna we are analyzing and m are the surrounding antennas producing coupling effects. Equations (2.7) and (2.8) consist of N integrodifferential equations, that is, one for every antenna, which contain the mutual coupling between the

antennas of the array. It results in N equations system with N $\mathbf{J_m}(\mathbf{r}'_m)$ unknown surface currents.

Recalling the planar arrays theory in [15], the main idea of the system of equations defined in (2.7) can be simplified. For 1D and 2D finite arrays, the surface current distribution can be defined as a weighted sum of a set of predefined distributions. For simplicity, in this case we consider that the current distribution is equal for all the conforming elements of the array. That is:

$$i_n(\mathbf{r}) = I_n f(\mathbf{r}) \tag{2.9}$$

where n is referred to the n^{th} element of the array, I_n is the weighted intensity coefficient and $f(\mathbf{r})$ is the current distribution. With the equation in (2.9), the unknown surface currents of the equation system have been replaced for a set of coefficients. The mutual coupling is now expressed by the following system:

$$V_m = \sum_m Z_{mn} I_n \qquad 1 \leq n \leq N \tag{2.10}$$

The mutual coupling produced by the m^{th} antenna to the analyzed n^{th} antenna is expressed by the impedance coefficient Z_{mn}. These coefficients connect the current amplitude I_n of each antenna with the applied voltages V_m to the ports. Thus, the impedance matrix built from this system of equations composed of Z_{mn} elements expresses the interaction between the antennas of the finite array. The equation (2.10) shows that the current is not just excited by the applied voltage, but also due to the incident field produced by the currents of the other surrounding elements. In the rare case of having a diagonal impedance matrix, this would mean that the array behaves as a set of isolated antennas.

2.3 Infinite arrays: Periodic Green's function

This section is especially focused on 2D infinite arrays explained in [15] and in [16] since in the thesis one of the main points will be the implementation of 3D Periodic Green's Function over 2D infinite arrays for rectangular and skew lattices.

As seen in figure 2.1, rectangular axes are a particular case for skew axes when $\varphi = 0°$. Thus, all the expressions related to skew lattice will be written only for the general case. In the infinite arrays, currents are proportional to the applied source. For periodic progressive sources, all currents are connected with a complex constant. In this case, all the antennas of the array are placed in the XY plane. The current distribution of an antenna port will be:

$$\mathbf{J}(\mathbf{r}_{nm}) = \mathbf{J}\left(x' + nd_s\cos\varphi, y' + md_y + nd_s\sin\varphi, z'\right) = \mathbf{J}\left(\mathbf{r}'\right)e^{-j\boldsymbol{\beta}_0\cdot\boldsymbol{\rho}_{nm}} \tag{2.11}$$

where

$$\begin{aligned} \boldsymbol{\beta}_0 &= \beta_{x0}\mathbf{x_0} + \beta_{y0}\mathbf{y_0} \\ \boldsymbol{\rho}_{nm} &= nd_s\cos\varphi\mathbf{x}_0 + \left(md_y + nd_s\sin\varphi\right)\mathbf{y}_0 \end{aligned} \tag{2.12}$$

$x = 0$ and $y = x\tan\varphi$ are the skew axes. d_s and d_y are the separation between elements in the skew and y axes, and $\boldsymbol{\beta}_0$ is the specified scan angle or phase shift. The expression in (2.11) is applied to the system of integrodifferential equations in (2.8) for the infinite array case. The complex term of the current can be included into the Green's Function in order to simplify the equation. Then, the infinite array is reduced to a single element with

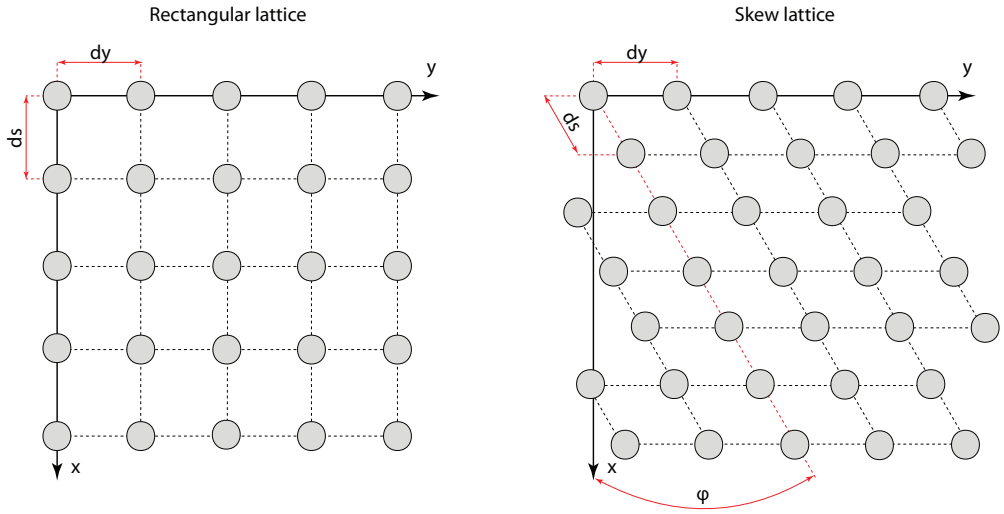

Figure 2.1: Rectangular and skew lattices

quasi-periodic boundaries. This is called Floquet Theorem. Every antenna will satisfy the same integral equation:

$$-\frac{j}{\omega}\widehat{\mathbf{n}}(\mathbf{r}_{pq}) \times V\delta(w)e^{-j\boldsymbol{\beta}_0\cdot\boldsymbol{\rho}_{pq}} = \widehat{\mathbf{n}}(\mathbf{r}_{pq})\times \\ \times\left(1+\frac{1}{k^2}\nabla\nabla\right)\left[\mu\sum_{mn}\iint_S G(\mathbf{r}_{pq},\mathbf{r}'_{nm})\mathbf{J}(\mathbf{r}')e^{-j\boldsymbol{\beta}_0\cdot\boldsymbol{\rho}_{nm}}\mathrm{d}\mathbf{r}'_{nm}\right] \tag{2.13}$$

Here the subindices p and q define the analyzed antenna and, n and m the surrounding antennas. In the equation (2.13) it is included the 3D Periodic Green's Function in a homogeneous media for 2D periodicity in free space:

$$G_p(\mathbf{r}) = \frac{1}{4\pi}\sum_{n=-\infty}^{+\infty}\sum_{m=-\infty}^{+\infty}\frac{e^{-jkR_{nm}}}{R_{nm}}e^{-j\boldsymbol{\beta}_0\cdot\boldsymbol{\rho}_{nm}} \tag{2.14}$$

where

$$R_{nm} = |\mathbf{r}-\boldsymbol{\rho}_{nm}| = \sqrt{(x-nd_s\cos\varphi)^2+(y-md_y-nd_s\sin\varphi)^2+z^2} \tag{2.15}$$

The equation (2.14) is a series with poor convergence $[O(1/n)]$, making it necessary to compute a large number of terms in order to obtain an accurate solution. In the next section, some transformations for accelerating the convergence are presented.

2.4 Acceleration techniques for the periodic Green's function

The 3D periodical Green's Function together with Floquet theorem reduce the infinite array structure to a single unit cell with quasi-periodic boundaries. The slowly convergent series is here transformed with some of the most relevant methods recommended in [16] for 2D periodicity. That is, the Edwald's method and the Poisson's summation formula, which is included inside the periodic Green's function accelerated with the first method.

Poisson's summation formula

The main idea here is that if in the spatial domain the 3D periodic Green's function has slow convergence, transforming the expression into the frequential domain the series will be faster. For that purpose the Fourier transformation is applied:

$$\sum_{n=-\infty}^{+\infty} f(\alpha n) = \frac{1}{\alpha} \sum_{p=-\infty}^{+\infty} F(\frac{2p\pi}{\alpha}) \tag{2.16}$$

Here $f(n)$ and $F(p)$ are the analyzed function in the spatial and spectral domain respectively, and α is a scaling factor. The expression in (2.16) is called Poisson Summation's Formula. Applying the transformation in the Periodic Green's Function (2.14) for skew lattice, yields :

$$G_p(\mathbf{r}) = \frac{1}{2jS} \sum_{n=-\infty}^{+\infty} \sum_{m=-\infty}^{+\infty} \frac{e^{-jk_z(n,m)|z|}}{k_z(n,m)} e^{-j\mathbf{k}_t(n,m)\cdot\mathbf{r}} \tag{2.17}$$

where

$$\begin{aligned} \mathbf{k}_t(n,m) &= \left(\beta_{x0} + 2\pi\left(\frac{n}{d_s\cos\varphi} - \frac{m\sin\varphi}{d_y\cos\varphi}\right)\right)\mathbf{x}_0 + \left(\beta_{y0} + \frac{2\pi m}{d_y}\right)\mathbf{y}_0 \\ k_z(n,m) &= \sqrt{k^2 - \mathbf{k}_t(n,m)\cdot\mathbf{k}_t(n,m)} \\ S &= d_s d_y \cos\varphi \end{aligned} \tag{2.18}$$

Here S is the area of the unit cell. The radiated plane waves, characteristic of the infinite arrays, can be clearly seen in the radiated electric field equation derived from the expression of the periodic Green's function in (2.17):

$$\mathbf{E}(x,y,z) = \sum_{n,m} \mathbf{C}_{nm} e^{-j[k_z(n,m)|z| + \mathbf{k}_t(n,m)\cdot\mathbf{r}]} \tag{2.19}$$

where C_{nm} is a complex vector. The terms of the sum in (2.19) are the Floquet modes. These modes, which can be TM or TE, are plane waves that propagate when $k_z(m,n)$ real, and evanescent when $k_z(m,n)$ imaginary. In 2D infinite arrays, the radiated field consists on a finite number of plane waves.

Edwald's method

This effective technique is used in particular when high accuracy is required. It is further explained in [17] and is based on the decomposition of 2D or 3D the Green's function using the following identity:

$$\frac{e^{-jkR}}{R} = \frac{2}{\sqrt{\pi}} \int_0^{\infty} e^{-R^2 s^2 + \frac{k^2}{4s^2}} \mathrm{d}s \tag{2.20}$$

The right side of the identity will be used to replace the periodic Green's Function in equation (2.14). The resulting integral is split in two parts. That is, from 0 to E and from E to ∞. Here, E is a parameter to be optimized and is related to the separation point between both integrals. The first integral will have the same convergence as the series without the transformation. For that reason, the Poisson's formula is applied. The second integral has fast convergence due to the Gaussian behavior. A singular point is present

when $R \to 0$, which belongs to the second integral. This singularity can be removed by extracting the problematic term because it is located in the spatial domain. However, this singular point will not be treated in the formulation below because it is irrelevant for the utilized MoM's code. In the case of the 3D periodic Green's Function with 2D periodicity, the decomposition will be:

$$G_p(\mathbf{r}) = G_{spectral}(\mathbf{r}) + G_{spatial}(\mathbf{r}) \tag{2.21}$$

where

$$G_{spectral}(r) = \frac{1}{4jS} \sum_{m=-\infty}^{+\infty} \sum_{n=-\infty}^{+\infty} \frac{e^{-j\mathbf{k}_t(m,n)\cdot\mathbf{r}}}{k_z(m,n)} \times \\ \times \sum_{\pm} e^{\pm jzk_z(m,n)} \mathrm{erfc}\left(\frac{jk_z(m,n)}{2E} \pm zE\right) \tag{2.22}$$

$$G_{spatial}(r) = \frac{1}{8\pi} \sum_{m=-\infty}^{+\infty} \sum_{n=-\infty}^{+\infty} \frac{e^{-j\mathbf{k}_0\cdot\boldsymbol{\rho}_{mn}}}{R_{mn}} \times \\ \times \sum_{\pm} e^{\pm jzkR_{mn}} \mathrm{erfc}\left(R_{mn}E \pm j\frac{k}{2E}\right) \tag{2.23}$$

The optimal E parameter is given by the following expression:

$$E = \max\left\{E_{opt}, \frac{\sqrt{k^2}}{2H}\right\} \tag{2.24}$$

where

$$E_{opt} = \sqrt{\frac{\pi}{d_s d_y \cos\varphi}} \tag{2.25}$$

Here E is the parameter which minimizes the total number of terms required for a given accuracy and H the maximum number for e^{H^2} so as to prevent the loss of significant digits. The second term of the right side of the equation in (2.24) is included in order to avoid cancellation errors between the two parts of the decomposition.

2.5 Method of Moments

The finite and infinite array problems discussed in the previous sections are based on the electric field integral equation (EFIE). A popular way to solve them is the Method of Moments relying on RWG basis functions. All the modifications will be made in the environment provided by the Makarov Matlab scripts, based in this theory [4,5]. Hence, we here review the general concept of the MoM's as well as the particular case for RWG subdomain functions.

General formulation

For the case of finite and infinite arrays, the equations in (2.8) and (2.13) can be simplified as:

$$L(\mathbf{J}) = \mathbf{V} \tag{2.26}$$

Here $L(\cdot)$ is a linear operator representing the integrodifferential operator, $\mathbf{J}$ is the unknown current distribution and $\mathbf{V}$ is the voltage excitation. The current distribution in an antenna port is approximated by a set of N different current distributions or basis functions:

$$\mathbf{J} = \sum_{n=1}^{N} I_n \mathbf{f}_n(\mathbf{r}) \tag{2.27}$$

N is the total number of basis functions $\mathbf{f}_n(\mathbf{r})$ and I_n the unknown weighting coefficient for the n^{th} basis function. Applying (2.27) in the equation (2.26):

$$\sum_{n=1}^{N} I_n L(\mathbf{f}_n(\mathbf{r})) = \mathbf{V} \tag{2.28}$$

The inner product is defined as follows:

$$\langle \mathbf{f}_m(\mathbf{r}), \mathbf{f}_n(\mathbf{r}) \rangle = \int_S \mathbf{f}_m(\mathbf{r}) \mathbf{f}_n(\mathbf{r}) \mathrm{d}\mathbf{S} \tag{2.29}$$

where $\mathbf{f}_m(r)$ is the test function. Applying the inner product to (2.28) we obtain:

$$\sum_{n=1}^{N} I_n \langle \mathbf{f}_m(\mathbf{r}), L(\mathbf{f}_n(\mathbf{r})) \rangle = \langle \mathbf{f}_m(\mathbf{r}), \mathbf{V} \rangle \tag{2.30}$$

which is equal to the equation in (2.10) for the mutual coupling. From the previous expression the following $N \times N$ linear system is obtained:

$$\mathbf{Z} \cdot \mathbf{I} = \mathbf{V} \tag{2.31}$$

The equation in (2.31) contains the relation between the impedance matrix, the intensity coefficients and the applied voltages. This method can be used for both scattering and radiation problems. However, this project will be entirely focused on transmitting antennas. The main advantage of the EFIE formulation is that it is applicable to both opened and closed surfaces. Some basic structures like wires cannot be solved using this formulation. These geometries can be represented using an equivalent model consisting on a thin plane strip. The procedure of method of moments particularized for RWG basis functions in [5] is applied to this situation and explained below.

RWG edge element's model

In this model, the antenna structure is discretized using a triangular grid. A set of special subdomain-type basis functions are defined and assigned to the nonboundary (interior) edges of the triangular meshed structure. These functions are designed specially for being suitable with the EFIE formulation. The basis functions implicitly enforces a continuous currents at the edges. That is, the surface current density representation will be free of line or point charges. For the n^{th} interior edge a vector basis function is defined as (see figure 2.2):

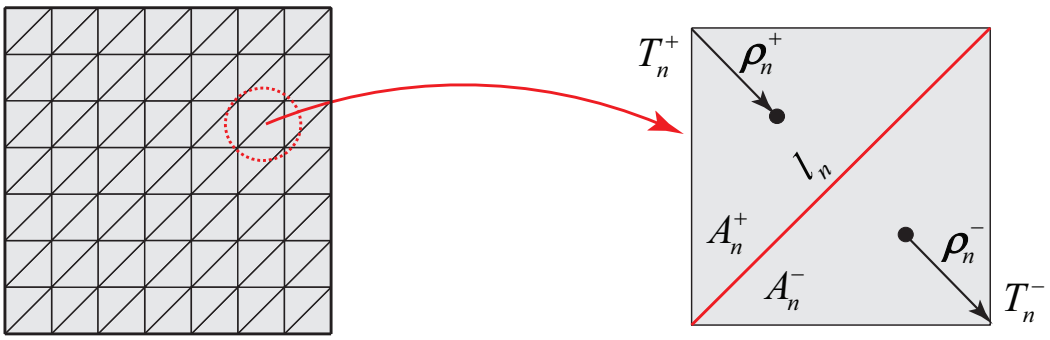

Figure 2.2: RWG model

$$\mathbf{f}_n(\mathbf{r}) = \begin{cases} \frac{l_n}{2A_n^+}\boldsymbol{\rho}_n^+ & r \text{ in } T_n^+ \\ \frac{l_n}{2A_n^-}\boldsymbol{\rho}_n^- & r \text{ in } T_n^- \\ 0 & \text{otherwise} \end{cases} \tag{2.32}$$

where l_n is the length of the edge, T_n^+ and T_n^- are the two triangles attached to the edge and $A_n^\pm$ is the area of $T_n^\pm$. $\boldsymbol{\rho}_n^+$ is the vector between the free vertex point of T_n^+ and its centroid point and $\boldsymbol{\rho}_n^-$ is the vector between the centroid point of T_n^+ and its free vertex point.

The testing procedure is applied to the EFIE equation (2.8, 2.13), using (2.32) as test functions. The Galerkin's Method is used to compute the coefficients of the matrix equation. In this method, the weighted functions and the basis functions are the same. Numerical integration approximations are used so as to eliminate the surface integrals present in the equation. Furthermore, they are perfectly suitable because the potentials in each edge are locally smooth. The approximation chosen for the observation point is given by the following expression:

$$\int g(\mathbf{r})\mathrm{d}S = \frac{A_m}{9}\sum_{k=1}^{9} g(\mathbf{r}_k^c) \tag{2.33}$$

where $g(\mathbf{r})$ is the Green's function and A_m is the area of the m^{th} triangle. It is called barycentric subdivision of an arbitrary shaped triangle. It consists of dividing the triangle into 9 small sub-triangles and supposing that the integrand is constant for every small triangle. Thus, $\mathbf{r}_k^c$ is the center point for the k^{th} subtriangle. The integral regarding the integration point is approximated by the centroid point of the triangle. Then, every impedance coefficient of the matrix is given by:

$$Z_{mn} = l_m\left[j\omega\left(\mathbf{A}_{mn}^+ \cdot \frac{\boldsymbol{\rho}_m^{c+}}{2} + \mathbf{A}_{mn}^- \cdot \frac{\boldsymbol{\rho}_m^{c-}}{2}\right) + \Phi_{mn}^- - \Phi_{mn}^+\right] \tag{2.34}$$

where the magnetic vector potential, $\mathbf{A}_{mn}^\pm$ is:

$$\mathbf{A}_{mn}^\pm = \frac{\mu}{4\pi}\left[\frac{l_n}{2A_n^+}\int_{T_n^+}\boldsymbol{\rho}_n^+(\mathbf{r}')g_m^\pm(\mathbf{r}')\mathrm{d}S' + \frac{l_n}{2A_n^-}\int_{T_n^-}\boldsymbol{\rho}_n^-(\mathbf{r}')g_m^\pm(\mathbf{r}')\mathrm{d}S'\right] \tag{2.35}$$

and the scalar vector, $\Phi_{mn}^\pm$ is:

$$\Phi_{mn}^{\pm} = -\frac{1}{4\pi j\omega\epsilon}\left[\frac{l_n}{A_n^+}\int_{T_n^+} g_m^{\pm}(\mathbf{r}')\mathrm{d}S' - \frac{l_n}{A_n^+}\int_{T_n^+} g_m^{\pm}(\mathbf{r}')\mathrm{d}S'\right] \tag{2.36}$$

The EFIE formulation solved with the MoM is useful for scattering and radiation problems. The excitation vector $\mathbf{V}$ will be different for each case. In this section, the problem is focused on transmitting antennas. The feeding model explained in the EFIE formulation is now applied, that is, the delta-function excitation in (2.5). The model assumes that the antenna structure is excited with a voltage gap of negligible width in which the voltage is V. In order to implement this model in the meshed antenna surface, this gap will be associated with just one nonboundary edge:

$$V_m = \begin{cases} l_n V & \text{for edge element } m = n \\ 0 & \text{otherwise} \end{cases} \tag{2.37}$$

Once all the coefficients of the impedance matrix and the voltage vector are solved, the system (2.31) can be solved in order to obtain the intensity vector $\mathbf{I}$ with the RWG weighted coefficients.

2.6 Array Scanning Method - Macro Basis Function method

The Method of Moments based on RWG basis functions can be employed on large meshed arrays. Then, the impedance matrix dimensions describing the mutual coupling between edge elements can be huge. This problem is caused because an unknown current coefficient is assigned for every edge. Thus, solving the resulting equation system usually requires a long computation time. This time can be reduced applying Macro Basis Functions (MBF). They are defined as a set of global functions for every antenna port including the whole subdomain functions defined on every antenna surface. This novel method reduces drastically the number of unknowns and the time spent for solving the equation system. In this project, the MBFs are obtained by the Array Scanning Method (ASM) for the case of 2D planar arrays. For completeness we recall the theory of MBFs and ASM following [4].

The current distribution on an infinite array is the superposition of the currents of the same array excited by a single antenna port. Furthermore, the surface current distributions of a finite array are almost the same as the current distribution in a infinite array, except at the edges. Having in mind the previous statements, the current distribution of a finite array can be expressed as the weighted sum of these currents. The ASM is utilized for extracting the infinite current distributions with only an excited antenna from the infinite array solution for different phase shifts. For a practical implementation, a DFT (Discrete Fourier Transform) approximation is used for the ASM. This approximation makes that the voltage excitation will be repeated every N antennas in both axis due to that approach. However, this will not affect to the final result because the current distributions are very similar.

Supposing that a 2D infinite array is excited every N antennas in both directions, the current on the port for the cell (m, n) is:

$$I_{m,n} = \frac{1}{N^2}\sum_{p=1}^{N}\sum_{q=1}^{N} I^{\infty}(\Psi_{s,p}, \Psi_{y,q}) e^{-jm\Psi_{s,p}} e^{-jn\Psi_{y,q}} \tag{2.38}$$

where

$$\Psi_{s,p} = \frac{2\pi p}{N} \quad \text{and} \quad \Psi_{y,q} = \frac{2\pi q}{N} \tag{2.39}$$

with p and q integers between 0 and $N-1$, and where $I^{\infty}(\Psi_s, \Psi_y)$ is the infinite-array current with inter-elements phasing of Ψ_s and Ψ_y along skew and y axis, respectively. The number of MBFs for the array solution will be N^2. That is, every distribution corresponding to an antenna of the infinite array excited every N antennas in both directions. N depends of the mutual coupling between elements, but a small number of MBFs is usually required.

The current distributions on the edge of the array are different from the inner area and this can lead to an inaccurate solution. For that reason, a small array with just edge cells (2×2) is fully solved in order to obtain the current distribution for this situation. That is, 4 MBFs that are added to the previous ones. Finally, the MBFs are orthogonalized using the Single Value Decomposition procedure (SVD) [18] so as to avoid an ill-conditioned system. This method decomposes the matrix in 3 more:

$$\mathbf{M} = \mathbf{S} \cdot \mathbf{V} \cdot \mathbf{D} \tag{2.40}$$

where $\mathbf{S}$ contains the orthogonalized basis. Depending on the desired accuracy, we can choose a certain number of MBFs from the whole set. A threshold is defined for this purpose. The number of MBFs chosen will be the number of singular values of the diagonal matrix, $\mathbf{V}$, above the defined threshold.

Finding the MBFs extracted from an infinite array is relatively quickly. We only have to solve a single cell with quasi-periodic boundaries and a small array. Hence, this method is clearly focused on solving problems with a smaller computational domain in order to be able to reduce the computation time.

Finally, the unknown current coefficients in the matrix equation system in (2.31) are replaced by a linear combination of the MBFs for every antenna:

$$\mathbf{J}_i = \sum_{m=1}^{R} \mathbf{I}_m \cdot \alpha_{im} = \mathbf{I} \cdot \boldsymbol{\alpha}_i \tag{2.41}$$

where R is the total number of MBFs, $\mathbf{I}$ represents the set of MBFs extracted obtained from the SVD procedure and $\boldsymbol{\alpha}_i$ is the vector containing the reduced set of unknowns for the i^{th} antenna. By following the procedure explained in [9], the matrix in (2.41) is applied to the impedance matrix describing the mutual coupling between the RWG elements of the array:

$$\mathbf{Z}^{MBF} = \begin{bmatrix} \left\langle \mathbf{J}_1^T, \mathbf{Z}_{11}^{RWG}, \mathbf{J}_1 \right\rangle & \left\langle \mathbf{J}_1^T, \mathbf{Z}_{12}^{RWG}, \mathbf{J}_2 \right\rangle & \cdots & \left\langle \mathbf{J}_1^T, \mathbf{Z}_{1N}^{RWG}, \mathbf{J}_N \right\rangle \\ \left\langle \mathbf{J}_2^T, \mathbf{Z}_{21}^{RWG}, \mathbf{J}_1 \right\rangle & \left\langle \mathbf{J}_2^T, \mathbf{Z}_{22}^{RWG}, \mathbf{J}_2 \right\rangle & \cdots & \left\langle \mathbf{J}_2^T, \mathbf{Z}_{2N}^{RWG}, \mathbf{J}_N \right\rangle \\ \vdots & \vdots & \ddots & \vdots \\ \left\langle \mathbf{J}_N^T, \mathbf{Z}_{N1}^{RWG}, \mathbf{J}_1 \right\rangle & \left\langle \mathbf{J}_N^T, \mathbf{Z}_{N2}^{RWG}, \mathbf{J}_2 \right\rangle & \cdots & \left\langle \mathbf{J}_N^T, \mathbf{Z}_{NN}^{RWG}, \mathbf{J}_N \right\rangle \end{bmatrix} \tag{2.42}$$

where

$$\left\langle \mathbf{J}_i^T, \mathbf{Z}_{ij}^{RWG}, \mathbf{J}_j \right\rangle = \boldsymbol{\alpha}_i^T \cdot (\mathbf{I}^T \cdot \mathbf{Z}_{ij}^{RWG} \cdot \mathbf{I}) \cdot \boldsymbol{\alpha}_j = \boldsymbol{\alpha}_i^T \cdot A_{ij} \cdot \boldsymbol{\alpha}_j \tag{2.43}$$

and to the vector describing the antenna excitations:

$$\mathbf{V}_i^{MBF} = \left\langle \mathbf{J}_i^T, \mathbf{V}_i^{RWG} \right\rangle \tag{2.44}$$

Here $\mathbf{Z}^{MBF}$ is the reduced impedance matrix, $\mathbf{Z}_{ij}^{RWG}$ the submatrix the mutual coupling between two antennas i and j, $\mathbf{V}_i^{RWG}$ is the excitation vector and $\mathbf{V}_i^{MBF}$ is reduced excitation vector for the i^{th} antenna. Therefore, the equation system in (2.31) is reduced to:

$$\begin{bmatrix} \mathbf{A}_{11} & \mathbf{A}_{12} & \cdots & \mathbf{A}_{1N} \\ \mathbf{A}_{21} & \mathbf{A}_{22} & \cdots & \mathbf{A}_{2N} \\ \vdots & \vdots & \ddots & \vdots \\ \mathbf{A}_{N1} & \mathbf{A}_{N2} & \cdots & \mathbf{A}_{NN} \end{bmatrix} \begin{bmatrix} \boldsymbol{\alpha}_1 \\ \boldsymbol{\alpha}_2 \\ \vdots \\ \boldsymbol{\alpha}_N \end{bmatrix} = \begin{bmatrix} \mathbf{V}_1^{MBF} \\ \mathbf{V}_2^{MBF} \\ \vdots \\ \mathbf{V}_N^{MBF} \end{bmatrix} \tag{2.45}$$

Considering that the 2D planar array consists of N different cells with M RWG basis functions for every antenna element, and that R MBFs have been employed, being $R \ll M$, the matrix dimension will decrease from $(N \times M) \times (N \times M)$ to $(N \times R) \times (N \times R)$. As it is a square matrix, it can be solved by LU decomposition. From the solved unknown weighted coefficients of the reduced matrix one can easily find the RWG unknowns coefficient. This coefficients can be extracted from the weighted sum of the MBFs for every antenna. That lead us to the solution for the original problem.

Chapter 3

Structure implementation of the MoM

The background code used in this project is introduced here. This code, developed by Makarov in [4], is aimed to solve both scattering and radiation problems for a great range of antenna geometries made of perfect electrical conductor. The program is based on the method of moments relying on RWG basis functions using the Galerakin's method for finding the full-wave solution. All the improvements will be implemented in the code included in chapter 4, which is focused on the radiation problems for one antenna.

In addition, a new script has been created for obtaining array meshes with rectangular and skew lattice from a basic antenna mesh file. The set of scripts included in the base program have also been modified in order to accelerate the construction of the impedance matrix and to introduce a phase shift in the y and skew directions. Finally, the accuracy of the the resulting code solutions has been tested here with a program based in the NEC2 code for a straightforward case.

3.1 A brief overview of the Method of Moment's code

The main goal of the code is to solve the basic parameters of the antenna structure such as the current surface distribution, the input impedance or the radiation pattern. For that purpose, the code is divided in two main parts: the first one obtains the surface current distribution from the file containing the mesh of the antenna and the second part solves the all parameters related to the near and far field. The modifications performed in this project are focused on the part of the program for solving the current over surface of the antenna.

A document with the mesh of the antenna structure is required in order to execute the first part of the code. Two vectors are needed to describe the mesh: $\mathbf{p}$, an array of $3 \times P$, and $\mathbf{t}$, an array of $4 \times N$. P and N are the total number of nodes and triangles for the antenna mesh, respectively. The first array, $\mathbf{p}$, describes the position in Cartesian coordinates of all the mesh nodes, and $\mathbf{t}$, includes the 3 nodes for every triangle of the mesh identified with a number. The fourth coordinate of $\mathbf{t}$ is used for working with non-planar antennas positioned in the XY plane, but here is not relevant because only planar antennas will be analyzed. These two arrays are enough to determine completely the meshed structure. This data can be obtained in several ways. One possibility is building the antenna with the *PDE toolbox* graphically, included in the Matlab software. It is also possible to define the mesh analytically with the Matlab functions *delaunay* or *delaunay3*, for 3D antennas. These functions are used, for instance,in the existing scripts included in the chapter 4 for modeling dipole strips of arbitrary dimensions and an specified number of edge elements.

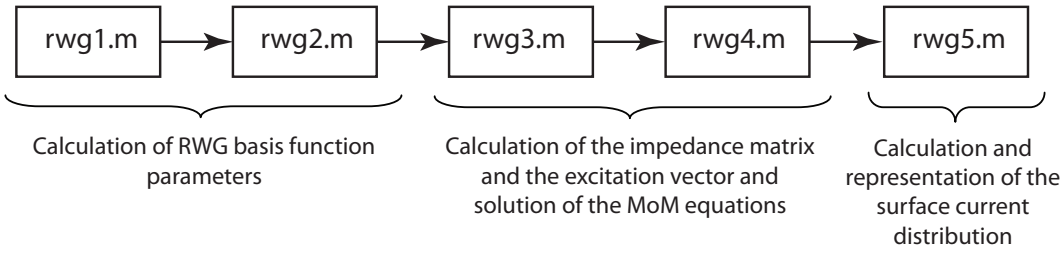

Figure 3.1: Flowchart of scripts for solving the surface current distribution of the analyzed antenna

The first part of the code consists of 5 different scripts (*rwg1.m*, *rwg2.m*, *rwg3.m*, *rwg4.m* and *rwg5.m*) which calculate the surface current of the structure. The file *rwg1.m* computes the basic parameters related to the triangles and edges of the antenna structure from the file containing the arrays $\mathbf{p}$ and $\mathbf{t}$. The 9 subtriangle midpoints and the area are found for every triangle in *rwg2.m* in order to perform the integral approximation by the barycentric subdivision. The vectors $\boldsymbol{\rho}^+$ and $\boldsymbol{\rho}^-$ are also defined in this script. Both scripts are used to obtain the basic parameters of the RWG basis functions required to calculate the coefficients of the impedance matrix. This matrix is built in the script *rwg3.m* using the function *impmet.m*. This function simplifies the system of integrodifferential equations with integral approximations based on the center point and the barycentric subdivision approaches. The vectorial formulation is also used for reducing the computation time of the coefficients. All the antennas analyzed here have the excitation in the origin $(0, 0, 0)$. Then, in *rwg4.m*, an algorithm assigns the feeding gap to the interior edge of the antenna closest to that point. The feeding vector is then built and finally, the vector of RWG current coefficients is obtained solving the system of equations $\mathbf{ZI} = \mathbf{V}$ with the function \ (backslash). As this impedance matrix is square, for a general case, the system will be solved by LU decomposition and performing a forward and backward substitution [19]. The current distribution on the antenna surface is represented graphically in *rwg5.m* . The inner edge coefficients in each triangle contribute to the final current distribution displayed. In figure 2, it is summarized the set of scripts explained above.

The second part is composed of 3 scripts (*efield1.m*, *efield2.m*, *efield3.m*). This code sequence calculates the field parameters from the surface current distribution obtained from *rwg5.m*. In *efield1.m*, the electric and magnetic fields are computed for an arbitrary observation point. The field magnitude is calculated over a large sphere in *efield2.m* and the radiation patterns for the E- and H-planes are solved in *efield3.m*. These 3 scripts are based on the function *point.m*. This function uses an approximation based in the dipole model [20]. This model considers that every inner edge of the antenna can be modeled as an infinitesimal dipole. The E- and H-fields are easily obtained because the dipole is a well-studied electromagnetic problem. The fields solution is found performing the sum of all the infinitesimal dipoles fields.

3.2 Implementation of a script for the creation of 1D and 2D arbitrary arrays

In this section, we have implemented a new script for creating arbitrary arrays from a single antenna mesh file. The MoM's code included in chapter 6 developed for Makarov includes a

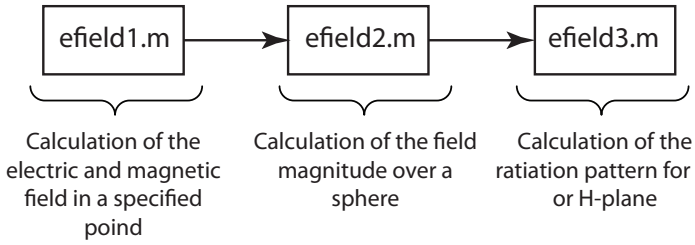

Figure 3.2: Flowchart of scripts for solving the radiation pattern in the E- or H-plane from the surface current distribution

file for performing this function. However, it is only useful for building 1D arrays. The new implemented script, called *array_creator.m*, can create 1D and 2D arrays with rectangular and skew periodicity. The existing script *rwg4.m* has also been modified for introducing a phase shift in both y and skew directions.

The script *array_creator.m* is a function with 4 input fields: number of antennas in the y and skew directions and the separation between elements in both axes. This function imports the mesh of a single antenna geometry containing the arrays $\mathbf{p}$ and $\mathbf{t}$. The skew angle is specified in the variable *skew*. The algorithm for creating the desired array from the antenna mesh consists of modifying the vectors $\mathbf{p}$ and $\mathbf{t}$ in order to include copies of the original antenna placed in the proper position. The 3D space coordinates for the nodes of the mesh, $\mathbf{p}$, are copied and added to the current vector with a displacement corresponding to the distance between the original and the current copy of the antenna. For instance, for a copied mesh in the row n and in the column m the displacement will be:

$$\mathbf{p} + (nd_s\cos(\varphi), md_y + nd_s\sin(\varphi), 0) \tag{3.1}$$

The vector containing the node numbers for every triangle, $\mathbf{t}$, is also copied and added to this vector. These new triangles do not have the same node numbers because the algorithm for creating the edge elements of the antenna array, present in *rwg1.m*, would compute wrong parameters. That is, the algorithm finds the edges by looking for a 2 common nodes for every pair of triangles. For instance, if two antennas had the same node numbers, inexistent edges would appear between these two. For that reason, the total number of nodes of the former cells is added to the node numbers of the copied antenna. This algorithm builds the array by rows. This fact is really important because affects to the structure of the impedance matrix.

An illustrative example for an 1D array with 1 row and 2 columns is presented in figure 3.3. The copied mesh has been displaced d_y in the y direction and the total number of nodes for the original mesh, 4, has been added to the new triangle components.

The script *rwg4.m* has also been modified for feeding all the antenna ports of the array. At the beginning of this script, we have defined 2 parameters for introducing a desired phase shift in both y and skew directions. The algorithm for assigning the excitation to the edge closest to the origin has also been changed. The origin point is now displaced according to the position of every antenna. Finally, the voltage vector construction has been modified for introducing the proper phase-shift in every port excitation.

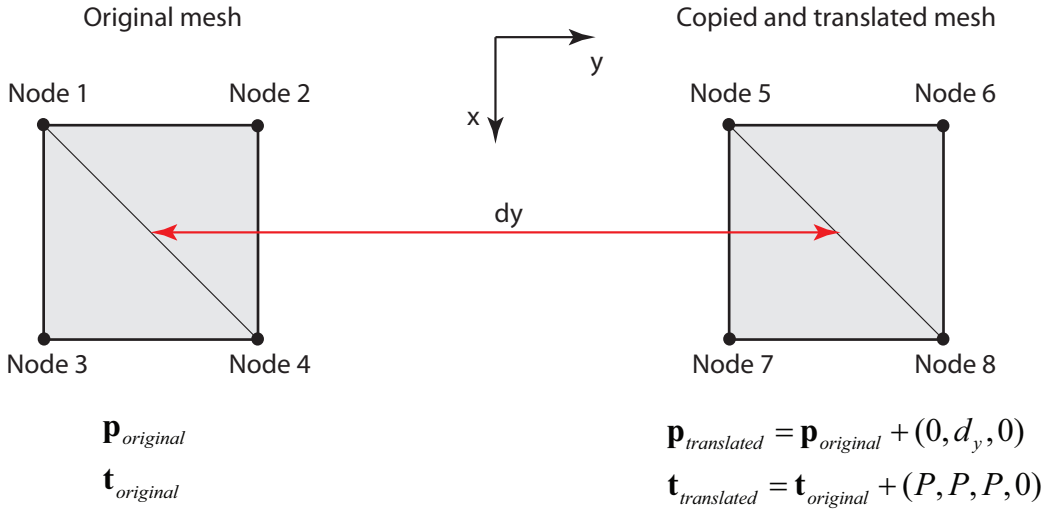

Figure 3.3: Illustrative example of the algorithm included in *array_creator.m* for the case of an array of 2 antennas positioned in the y axis

3.3 Implemented modifications for improving the efficiency of *impmet.m*

The mutual coupling between two edge elements is described by the mutual impedance. The reciprocity theorem states that the impedance coefficients Z_{12} and Z_{21} are equal when analyzing antennas made of PEC in a linear and isotropic medium [2], vacuum in the present project. Then, the coefficients of the impedance matrix describing the interaction between two edge elements must be equal. The previous theorem assures that the impedance matrix containing the mutual coupling effects for the edge elements is symmetric. However, this reciprocity is not fulfilled for the used code. For instance, the crossed coefficients for the first and second edge of an antenna are not exactly the same:

$$\begin{aligned} Z_{12} &= -0.0002 - j0.7524 \\ Z_{21} &= -0.0002 - j0.7439 \end{aligned} \tag{3.2}$$

A dipole strip of $\lambda/2$ working at 75 MHz with 39 edge elements and the geometric dimensions described in (3.3) has been used in this example. This problem is caused due to the algorithm that builds the impedance matrix, implemented in *impmet.m*. For every triangle of the antenna structure, this script looks for all the nonboundary edges. Depending whether the triangles belongs to T^+ or T^-, the part of the impedance coefficients that are calculated from T^+ or T^- are computed with respect to the rest of the edges of the structure. The coefficients are computed by sweeping all the triangle of the mesh, but not at once. The integrals included in the integrodifferential equation for computing the mutual coupling are approximated. The integral affecting the analyzed edge is approximated by the triangle center point and the other affecting the edge producing the coupling effect is approached the barycentric subdivision. Hence, the reciprocity is broken because the integral approximations are different depending on the reference edge.

The impedance matrix contains several redundancy when arrays of symmetric antennas are analyzed. The algorithm for the construction of this matrix does not take into account that fact because it is implemented for a general case. For that purpose, the script *impmet.m*

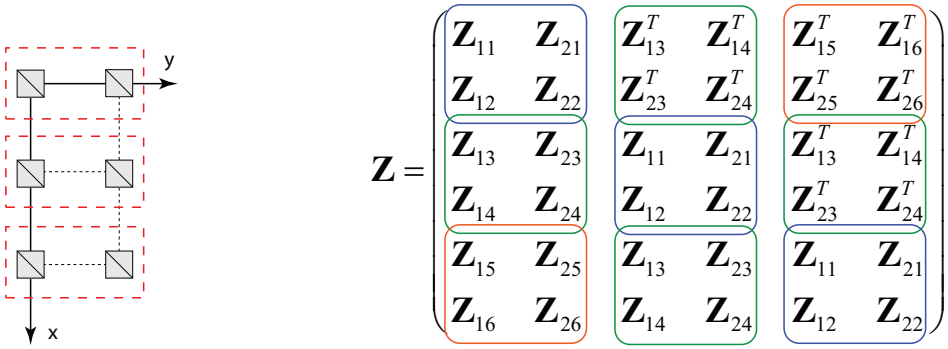

Figure 3.4: Example of a 2D planar array with 3 rows and 2 columns. The resultant impedance matrix is Toeplitz-symmetric with the blocks above the diagonal transposed. Every block is a submatrix containing the mutual coupling effects of a sub-array of 2 antennas. The number of antennas considered inside a sub-array is the number of the array columns

has been modified. A 2D array is generated from a single antenna mesh file, building the mesh by rows. The matrix is not symmetric because of the integral approximations. Then, the redundancy is present at the level of sub-arrays of antennas instead of at the edge elements level. If the array is subdivided in R sub-arrays of Q antennas, where R is the number of rows and Q is the number of columns, the mutual coupling between these sub-arrays will be reciprocal. This means that the impedance matrix will be Toeplitz-symmetric matrix of $Q \times Q$ sub-matrices with dimensions $(R \times S) \times (R \times S)$, where S is the total number of edge elements per antenna.

We have created an algorithm that exploits this property in order to accelerate the construction of the matrix. The structure of the a Toeplitz-symmetric matrix can be built from only one column. Thus, computing only the impedance coefficients between the first sub-array with and rest of the array is enough for building the whole matrix. Furthermore, the mutual coupling effect between a given antenna and the left-side one is not he same that with the right-side one. That is, the effect produced in the right part in one antenna is the same that in the left part of the other one. The new algorithm transposes the blocks located in the upper-triangle of the matrix for solving this problem. In figure 3.4, the algorithm is shown for an array with 3 rows and 2 columns in the skew and y directions, respectively. The new script considers this array as a new one with only 3 antennas in the x axis. With the computation of the first column of blocks (blue, green and red), the impedance matrix is completely determined.

The efficiency of the modified script has been tested for 3 different cases: Rectangular lattice in the broadside direction, skew lattice ($\varphi = 30°$) in the broadside direction and rectangular lattice with a phase-shift of $\pi/4$ in the y direction. The periodicity in all cases is $\lambda/2$ and $3\lambda/4$ in the skew and y axes respectively. The antenna chosen for this purpose is a dipole strip of $\lambda/2$ (figure 3.8) with the following parameters:

$$\begin{aligned} l &= \lambda/2 = 2 \text{ m} \\ w &= 0.02 \text{ m} \\ f &= \frac{c}{\lambda} = 75 \text{ MHz} \end{aligned} \tag{3.3}$$

where l is the length of the dipole, w is the width of the strip and f is the working frequency.

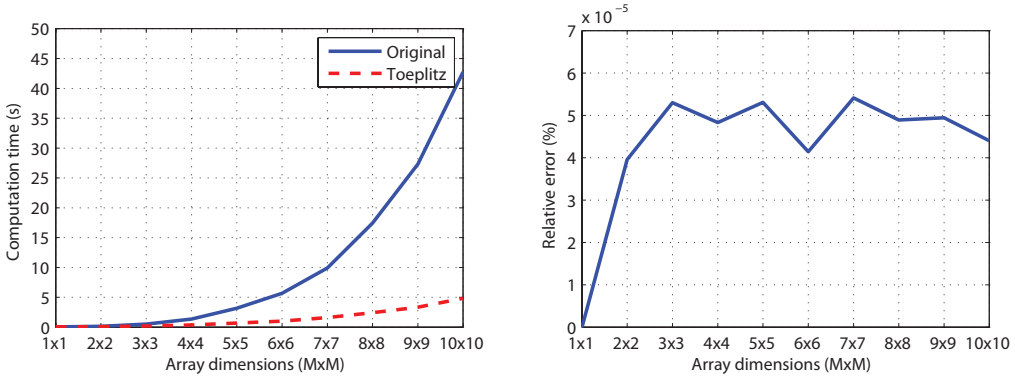

(a) Comp. time of the imp. matrix construction

(b) Max. relative error of the input imp.

Figure 3.5: Evaluation of the improvement based on the Toeplitz-symmetric property. An array of dipoles for rectangular lattice in the broadside direction is considered here for different dimensions

The antenna has been discretized with 39 non-boundary edge elements. The dipole is the simplest and most well-studied antenna structure. For that reason, almost all the new implementations presented in this project will be verified with this straightforward case. For all the cases the computation time and the relative error have been analyzed for different array dimensions. Here the relative error is defined for the input impedance in all the antenna ports. The reference values are obtained from the original set of scripts. The represented value corresponds to the worst case. As shown in figures 3.5, 3.6 and 3.7, the computation time and the relative error do not differ in the 3 cases analyzed. The computation time with the new algorithm decreases proportionally to the number of computed terms. That is, the time reduction for an array of $M \times M$ dimensions is around $1/M$ because it is only necessary to compute a $1/M$ part of the whole impedance matrix. The relative error is always below $10^{-4}\%$. This result verifies that the error produced by the modification implemented is negligible compared to the error introduced by the discretization of RWG basis functions and the integral approximation, as we will see in the next section.

3.4 Example: 2 dipole antennas of $\lambda/2$ in transmission mode

The basis MoM's code with the modifications explained in the previous sections is now tested for a array of 2 dipole antennas of length $\lambda/2$ with a separation distance in the y axis of $\lambda/2$ and with the same parameters that in section 3.3 (figure 3.8). Both antennas work in transmission mode and are excited with 1 V in broadside configuration. The obtained results will be compared with the *4nec2* software. This program uses the Numerical Electromagnetics Code (NEC-2), which is based in the numerical solution of integral equations (EFIE for surfaces and MFIE for wires) using the MoM [21,22].

The *4nec2* software work with wires instead of strips for modeling dipoles. The equivalent cylindrical radius for a given strip is approximated with the following expression [3]:

$$R_{eq} = 0.25w = 0.005 \text{ m} \tag{3.4}$$

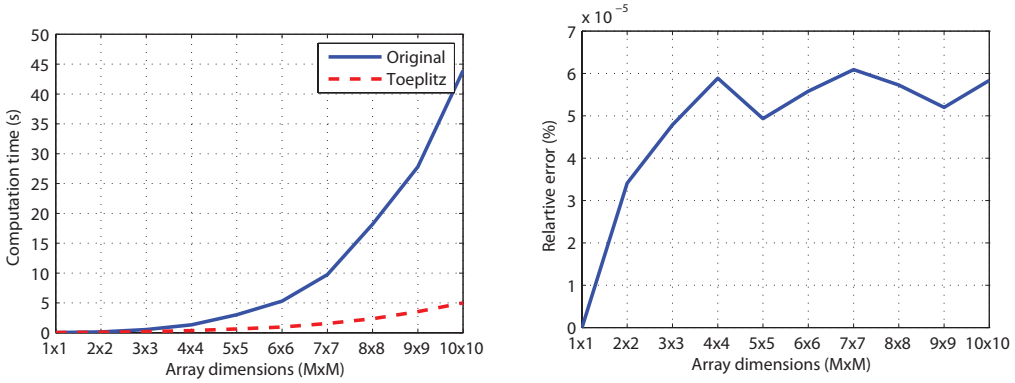

(a) Comp. time of the imp. matrix construction (b) Max. relative error of the input imp.

Figure 3.6: Evaluation of the improvement based on the Toeplitz-symmetric property. An array of dipoles for skew lattice with $\varphi = 30°$ is considered here for different dimensions

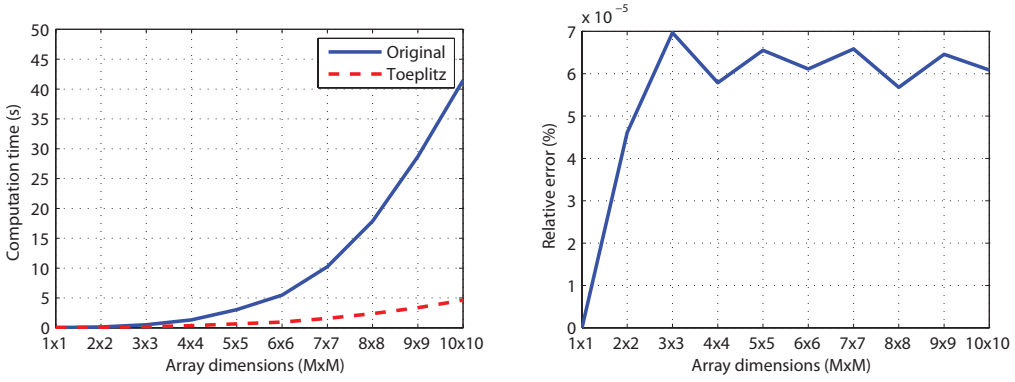

(a) Comp. time of the imp. matrix construction (b) Max. relative error of the input imp.

Figure 3.7: Evaluation of the improvement based on the Toeplitz-symmetric property. An array of dipoles for rectangular lattice with $\pi/4$ of phase-shift in the y axis is considered here for different dimensions

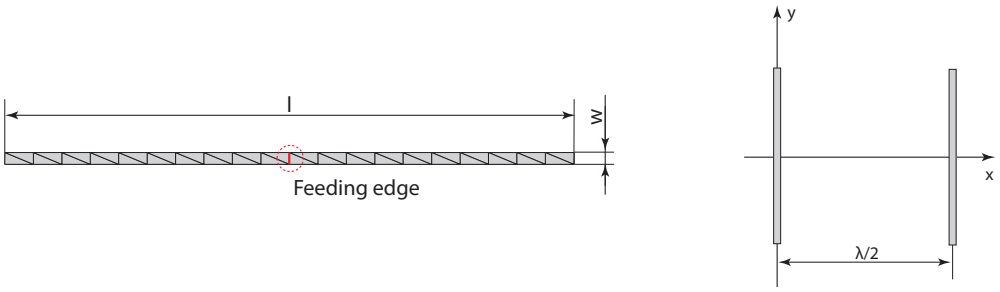

Figure 3.8: Representation of the dipole strip geometry and the array analyzed in the example

	Makarov's code	**NEC2**	**Relative error (%)**
Input impedance (Ω)	$66.9121 + j10.3093$	$66.6 + j16.4$	1.3
Gain(dB)	5.9086	6	1.5

Table 3.1: Simulated parameters for the array of 2 dipoles with the MoM's code and the NEC2 software. The relative error is referenced with the NEC2 results

where w is the width of the strip. The sequence of scripts computing the surface current distribution and the radiation pattern have been executed. In table 3.1, the input impedance, which is the same for both antennas ports, and the gain of the array are presented. The same parameters have been computed with the *4nec* program, which have been considered as the reference values. The relative error is around 1% in both analyzed cases showing good accuracy when dipoles of 39 edge elements are used.

The radiation patterns for E-plane and H-plane are presented in figure 3.9. The results obtained from the modified code match perfectly with the NEC2 software. Hence, a good accuracy is achieved for this array despite the integral approaches already implemented in the original code and the new modifications.

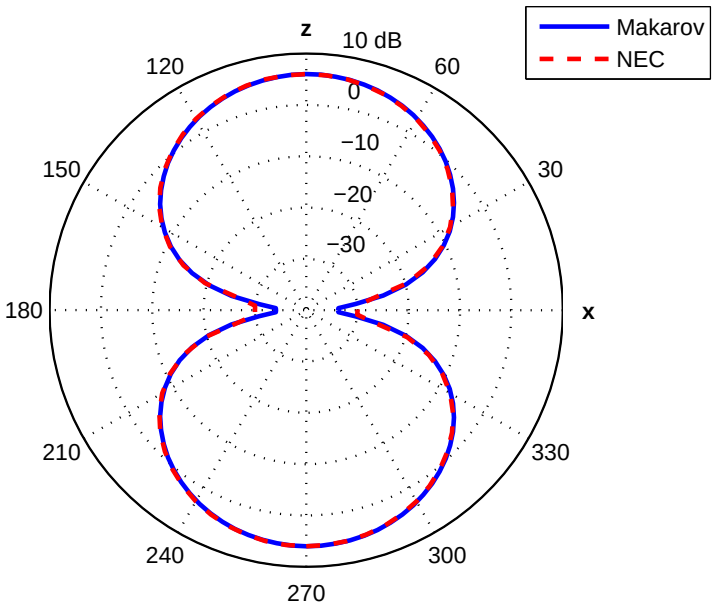

(a) E-plane radiation pattern

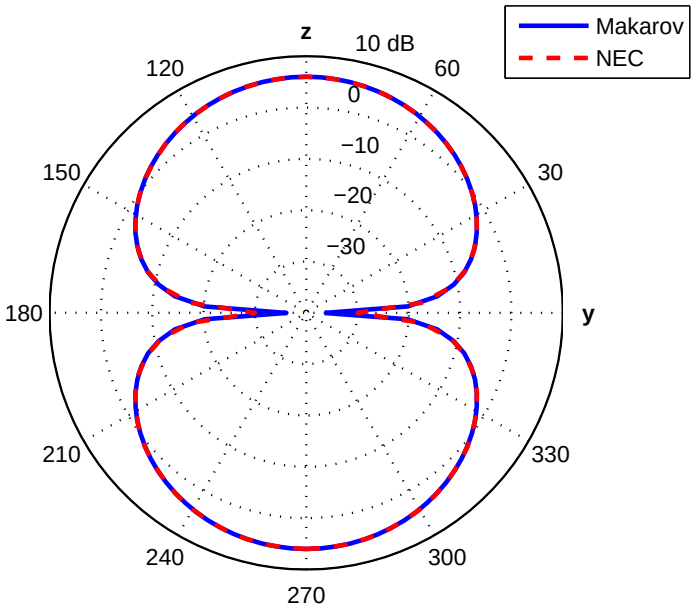

(b) H-plane radiation pattern

Figure 3.9: Comparison of E- and H-plane radiation patterns between the MoM's code and *4nec2* program for the array of 2 dipoles

Chapter 4

Implementation of a code for solving 2D infinite planar arrays

The MoM's code is modified here in order to solve the surface current distributions in 2D planar infinite arrays with both rectangular and skew lattices and for an arbitrary scanning angle. In the background theory, it was mentioned that by applying the Floquet theorem, an infinite array can be expressed as a single antenna cell with quasi-periodic boundaries. The 3D Green's function inside the integrodifferential equations is then transformed into the 3D periodic Green's function. This expression is a very slowly convergent series. For that reason, some acceleration methods recommended for this case are analyzed in terms of convergence, accuracy and computation time. The singularities of the accelerated periodic Green's functions and the limitations produced are also discussed. Finally, the best expression is implemented in the basis code. The results are verified with a software based on finite-difference time-domain method (FDTD).

4.1 Justification of the Edwald's Method as the proper acceleration method

The 3D periodic Green's function and the best technique for acceleration its convergence are analyzed in [16]. The Edwald's method is mentioned as the most effective for the case of 2D periodicity, especially when a high accuracy is required. In this section, this accelerated expression is analyzed and compared with other expressions of the function so as to verify the properties of this transformation. We have created a Matlab script containing 3 different expressions of the periodic Green's function: The original one (2.14), included in the EFIE equation transformed with the Floquet theorem, the function accelerated with the Poisson's summation formula (2.17) and accelerated with the Edwald's method (2.21). The Poisson's accelerating method is demonstrated in the reference paper [16] as an ineffective technique for the analyzed situation. However, it is part of the Edwald's derivation.

The Edwald's expression can not be implemented with predefined Matlab functions because the complementary error function included is not compatible with complex arguments. In [23], it is implemented a script that computes the Fadeeva function using rational series with N terms. We have implemented a new script for computing the complementary error function from the Fadeeva function considering that:

$$\mathrm{erfc}(x) = \begin{cases} e^{-x^2}\omega(jx) & \mathrm{Re}(x) \geq 0 \\ 2 - e^{-x^2}\omega^*(jx^*) & \mathrm{Re}(x) < 0 \text{ and } \mathrm{Im}(x) < 0 \\ 2 - e^{-x^2}\omega(jx) & \mathrm{Re}(x) < 0 \text{ and } \mathrm{Im}(x) \geq 0 \end{cases} \tag{4.1}$$

where $\omega(x)$ is the Fadeeva function. The number of terms chosen for this function introduces a trade-off between the accuracy and the computation time. 20 terms are enough for solving the complementary error function with a relative error less than $10^{-12}\%$ without affecting excessively the computation time.

The convergence, computation time and accuracy of the 3 periodic Green's functions are now tested in order to verify which expression has better properties in the unit cell region located in the origin of coordinates. The 3 expressions are analyzed without considering the EFIE equation in which are included. That is, it is only taken into account the 2D periodical space in the xy plane without any antenna. First of all, the behavior of the 3 functions is checked along the xy plane and the z axis. For the xy plane we have considered a working frequency of 75 MHz because the dipole antenna used in the following sections works at this frequency. The periodicity specified in both x and y axis is $\lambda/2$ in figure 4.1 (a) and $3\lambda/4$ in figure 4.1 (b). These 2 examples are shown for assuring the conclusions extracted from the plots. In both figures, all the expressions have been swept along $x = y$ and z = 0 for the broadside case. The total number of computed terms is 25 for the 3 functions. The reference value is computed from the Edwald's method expression for 121 terms because according to the reference paper [16] it is enough for having an excellent accuracy. The relative error is extracted from the following formula:

$$\epsilon(\mathbf{r}) = \frac{|G_{reference}(\mathbf{r}) - G_{tested}(\mathbf{r})|}{|G_{reference}(\mathbf{r})|} \times 100 \tag{4.2}$$

where $G_{reference}(\mathbf{r})$ is the reference value of the periodic Green's function for a given observation point and $G_{tested}(\mathbf{r})$ is the value analyzed for the 3 expressions. Both figures show that the 3D periodic Green's function has singularities in $\mathbf{r} = (nd_s, md_y, 0)\ \forall m = n$. These singular points are produced due to the singularity of the 3D Green's function located at the origin. This fact will not affect to the solution of an infinite array problem because the cell area only includes the singularity at the origin. However, even for the worst case of computing the self-coupling of an edge, the periodic Green's function will not be evaluated at this singular point. The integrodifferential equation for the RWG basis functions uses different approximations for the 2 integrals, the centroid point and the 9 point approach. This means that the reference and the observation points will be different for every approximation and the resultant distance will not be zero. The original expression and the expression accelerated with Poisson's summation formula have bad accuracy in the entire region analyzed. When $z = 0$, the value of the additional exponential term that contains the Poisson's expression is equal to 1, having approximately the same convergence that the original expression. The Edwald's expression loses accuracy when the distance from the origin increases. Taking into account that the region of the cell has the size of the periodicity, the relative error will be kept below $10^{-4}\%$.

The convergence of the 3 expressions of the 3D periodic Green's function has also been evaluated along the z axis in figure 4.2 for a periodicity of $\lambda/2$ in both directions, considering the broadside case. We have considered this periodicity because it has been already analyzed for the xy plane. The coordinates of the observation point are determined for a general case inside the unit cell area. That is, $x = \lambda/4$ and $y = \lambda/8$. The evaluated and reference values for the periodic Green's functions have been obtained in the same manner that in the previous plots. For z = 0, the relative error of the Poisson's expression is the almost

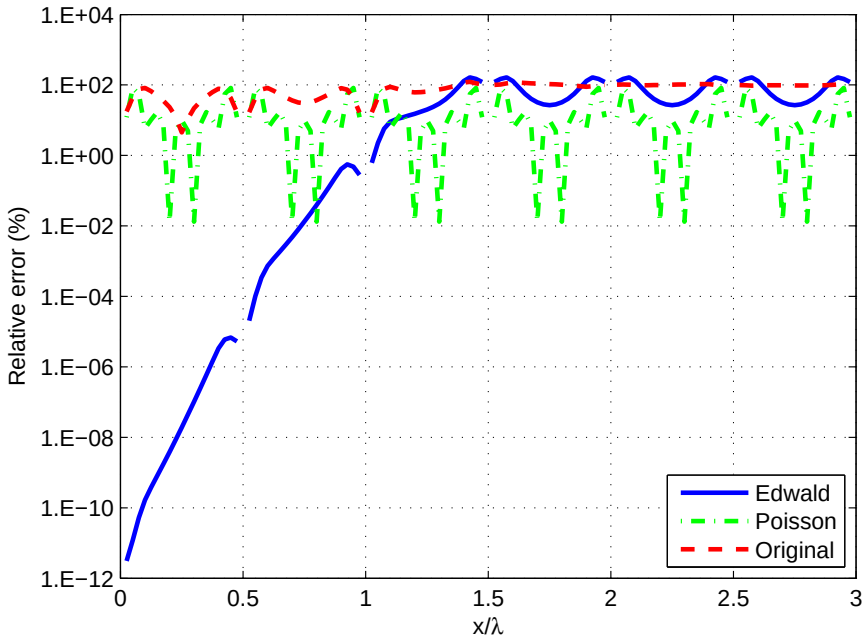

(a) Periodicity of $\lambda/2$ for both x and y axis

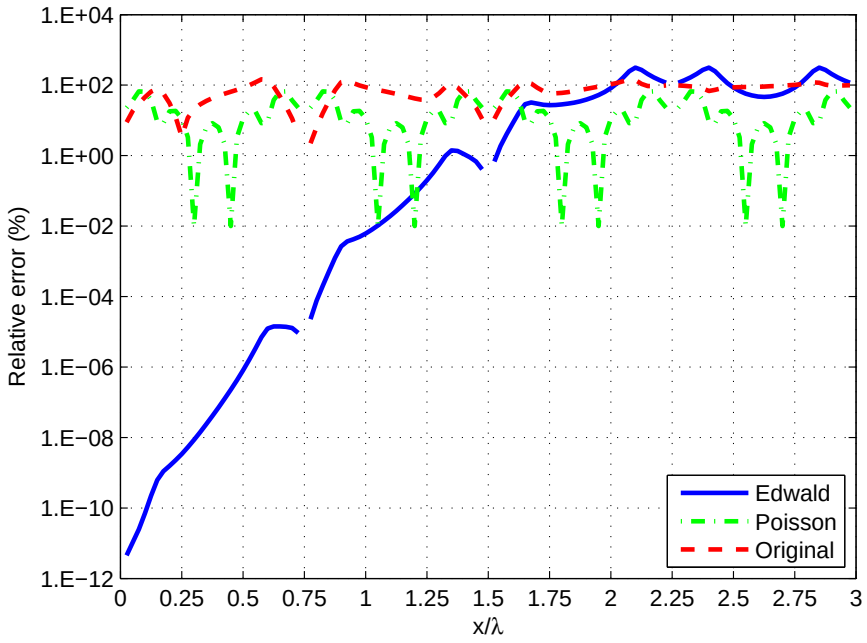

(b) Periodicity of $3\lambda/4$ for both x and y axis

Figure 4.1: Relative error of the 3 expressions of the 3D periodic Green's function for x=y and z=0 computed for 25 terms. The relative error is referenced with the Edwald's expression for 121 terms

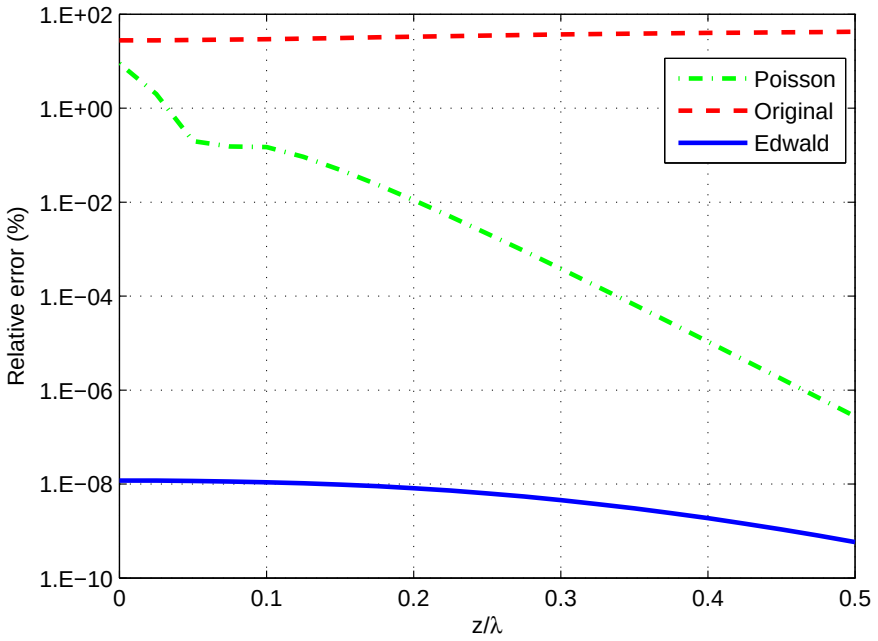

Figure 4.2: Relative error of the periodic Green functions achieved as a function of z for a given coordinates $x = \lambda/2$ and $y = \lambda/8$. All the expressions are computed for 25 terms. The Edwald's expression for 121 term is used as reference value

the same that the original one, verifying the conclusions extracted from the previous plots for the xy plane. As z increases, the convergence is accelerated until reaching a relative error only 2 orders of magnitude over the Edwald's expression. This effect is produced because the exponential term included in the function accelerated with Poisson tends to 0 as the value of z becomes larger. The relative error of the original expression is huge for all the swept points due to the slow convergence of the series. The relative error of the Edwald's method is in this case always equal or below $10^{-8}\%$, which can be considered negligible. The results shown in figures 4.1 and 4.2 verify that the 3D periodic Green's with the Edwald's method is the best technique for accelerating the convergence in case of considering 2-dimensional periodicity.

The Edwald's method has been verified as the most effective in terms of convergence. The last property to analyze in order to assure our decision is to evaluate the relative error of the 3 expressions depending on the computation time and the total number of computed terms. The working frequency is 75 MHz, the periodicity is λ in both d_s and d_y and the scanning angles are $\theta = \phi = 45°$. The observation point chosen for this case is $\mathbf{r} = (\lambda/4, \lambda/8, \lambda/8)$ because the analyzed point represents a general case inside the area of the cell placed in the origin. Furthermore, the Poisson's expression is not tested in the worst case, that is, when $z > 0$. In this case, the reference value of the periodic Green's function is obtained from the computation of the Poisson's expression with 2000 terms [24]. In figure 4.3 (a) the relative error of the 3 expression are obtained for different computed terms. As it was expected from the previous results and the reference papers mentioned in this section, the Edwald's function has the faster convergence reaching a relative error of

10^{-7}% for just 50 terms. The Poisson's expression needs 1000 terms for reaching the same relative error. The original expression has very slow convergence being necessary more than 10^5 terms to reach a relative error of 1 %. The computation time is shown in figure 4.3. (b) for the same case. The function accelerated with Poisson is faster for a relative error bigger than 10^{-1} due to the delay introduced by the computation of the complementary error function. However, we will choose the expression accelerated with Edwald's method with 50 terms because a high accuracy is reached for less time even when the Poisson's expression is not evaluated for $z = 0$, the worst case. That is, when the convergence is not the same as the original expression.

4.2 Implementation of the 3D periodic Green's function in the MoM's code

The 3-dimensional periodic Green's function accelerated with the Edwald's method has been verified as the expression with the best properties in terms of convergence and accuracy inside the cell area where the antenna will be located. In this section, we have implemented this function in a new script, *edwald_skew.m*, with 50 computed terms. The 3D Green's function included in *impmet.m*, where the impedance matrix is built, has been replaced by the new script. We have used the same code for the periodic Green's function accelerated with the Edwald's method that in the previous section. Whereas, we have modified the complementary error function for complex arguments. *edwald_skew.m* has to work with vectors containing all the observation points for all the subtriangle midpoints of the antenna respect to the analyzed triangle. For that reason, the script *cerfc.m* has been replaced by *Merfc.m*. The 3 different functions containing the erfc(x) for complex arguments are compatible with vectors. However, for the same vector, some values have to be computed with a different functions of the erfc(x), which is impossible to do with the *cerfc.m*. In the Edwald's expression, the input value of the complementary error function belongs to all the complex space except for the 3$^{\text{rd}}$ quadrant. This means that only 2 of the 3 functions forming the erfc(x) are used here. The algorithm of the new script will compute the expression for the 4$^{\text{rd}}$ and 1$^{\text{st}}$ quadrant for all the values. This can be seen in equations (2.22) and (2.23) when $z = 0$, which is the most common situation. The values belonging to the 2$^{\text{nd}}$ quadrant are replaced individually as they are a rare case for the planar antennas analyzed in this project. The script *edwald_skew.m* can work with both rectangular and skew lattices and with an arbitrary scanning angle.

The modified MoM's program for analyzing 2D infinite planar arrays in the xy plane is now verified for a simple case. A dipole antenna of $\lambda/2$ oriented in the y axis (figure 3.8) has been chosen for this case. The working frequency is 75 MHz, and it has been considered a rectangular lattice with periodicities of $\lambda/2$ and $3\lambda/4$ for x and y axes respectively in the broadside direction. The convergence of the input impedance has been evaluated depending on the total number of edge elements employed for discretizing the surface of the dipole strip. For obtaining the relative error, the reference values has been calculated with the PBFDTD software [25] based on the FDTD method. This method discretizes the volume of the cell. The Maxwell equations in partial differential form and time-dependent are applied to a sample of volume in a given instant time for solving the electric field. The magnetic field is solved in the next instant of time. In this case, the obtained input impedance was $55.2874 - 5,2112j(\Omega)$. As it is shown in the figure 4.4, the relative error reaches a minimum under the 2% for 119 edge elements and it remains belows the 4% when the mesh is further refined. One must take into account that the dipole simulated in the PBFDTD is an approximation of the the dipole strip. That is, the length and the radius is not the

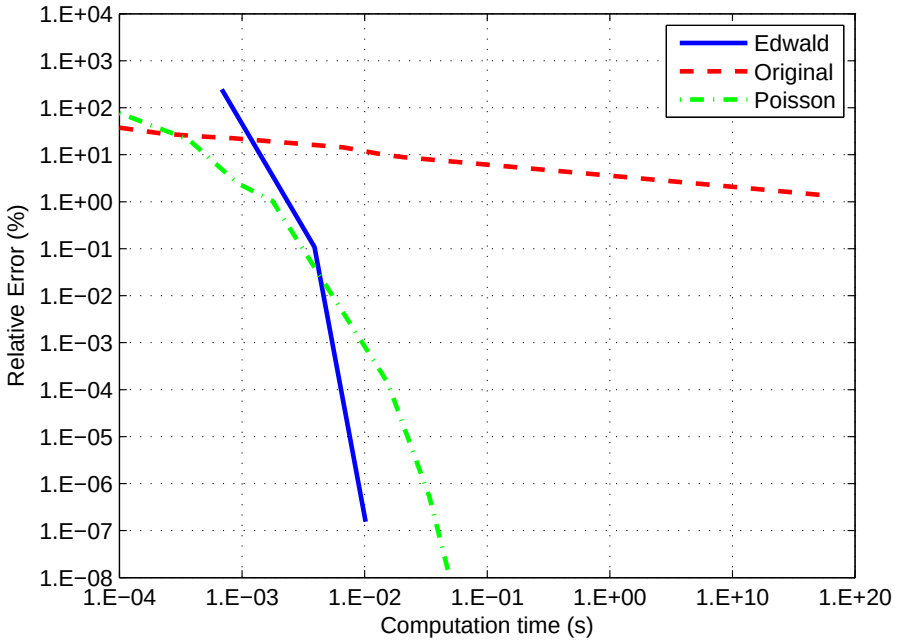

(a) Relative error achieved for a certain computation time

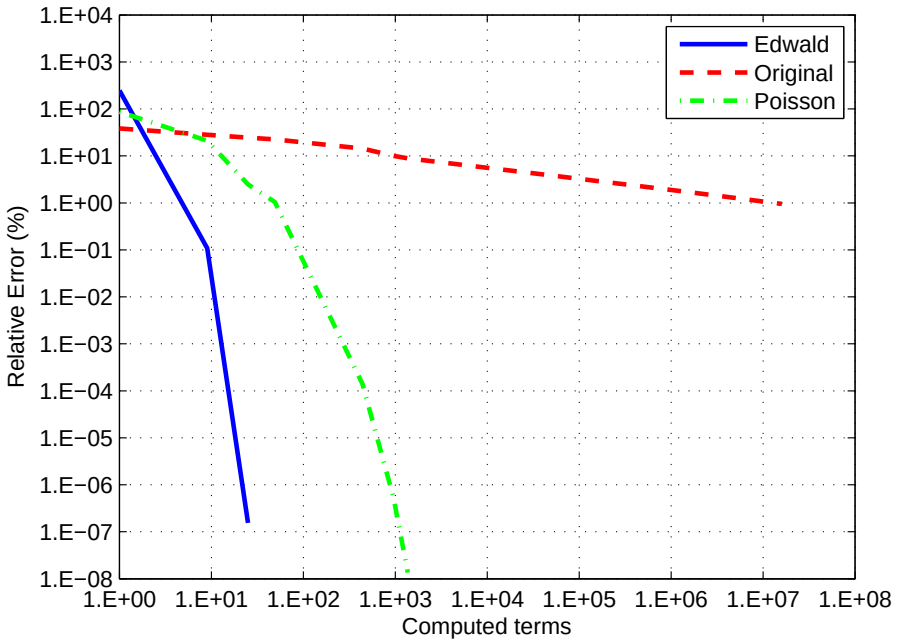

(b) Relative error achieved for a certain number of computed terms

Figure 4.3: Relative error for the 3 expressions of the 3D periodic Green's function. In this case, the reference value is obtained from the Poisson's expression for 2000 computed terms

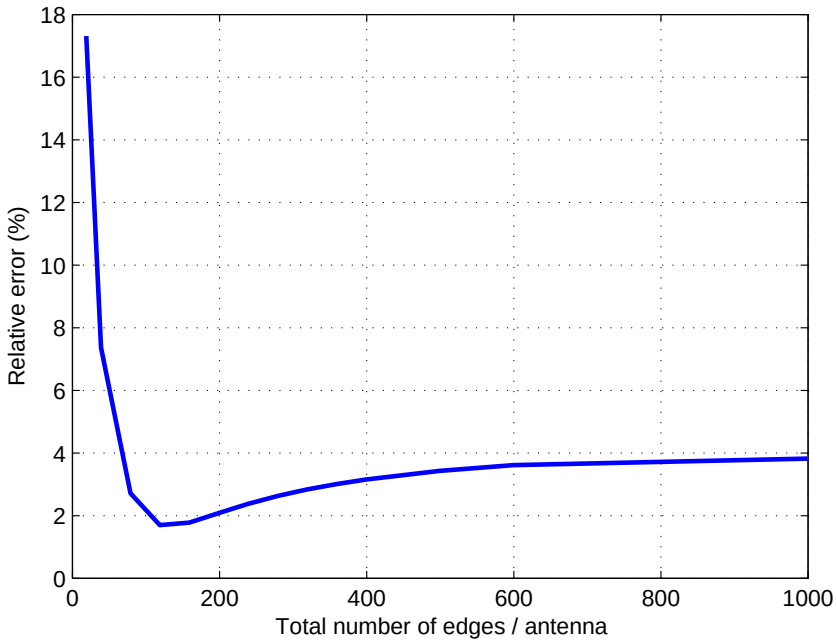

Figure 4.4: Evaluation of the convergence of the input impedance for the number of RWG edge elements used to model an infinite array of dipoles of $\lambda/2$. The periodicities considered here are $\lambda/2$ and $3\lambda/4$ in the skew and y directions with rectangular lattice in broadside direction.

same because the volume of the cell is discretized without having a perfect accuracy. This can be the reason why the relative error slightly increases after reaching the minimum. The total number of edge elements chosen for the following verifications is 119.

In figure 4.5, the program that we have implemented is verified for the previous dipole antenna with the same periodicities. The real and imaginary parts of the active reflection coefficient are obtained for a range of scanning angles (from $\theta = 0°$ to $90°$) in the E-plane ($\phi = 0°$) and the H-plane ($\phi = 90°$). The obtained values match perfectly with the reference results from PBFDTD software in both plots. The poor sampling of the reference data is produced due to impossibility of solving the problem for more than one scanning angle every simulation. The real part of the active reflection coefficient in the E-plane for $75°$ does not coincide. The FDTD method converges to the solution by iterating. Sometimes the solution become unstable after many iterations, especially for large angles from broadside direction, as the analyzed case [26].

The code developed in this section is now evaluated for an example with skew lattice in figure 4.6. The same dipole antenna is used for an infinite array with triangular lattice. This lattice is a special case of skew periodicity in which the distance between antennas in the y and skew directions is the same and the skew angle is $\varphi = 30°$. In this case, the periodicity is $3\lambda/4$ in both directions. The real and imaginary parts of the active reflection coefficient of the antenna are simulated for the same case that in the rectangular lattice. In both E-plane and H-plane, the results agree well despite the apparent grating lobe present in both figures. The imaginary part of the active reflection coefficient for $\theta = 40°$ in both

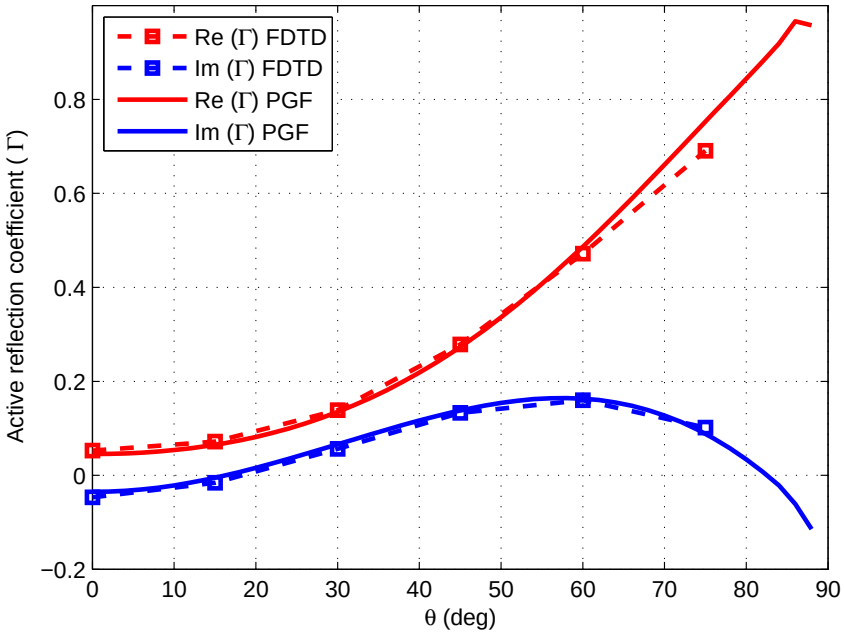

(a) E-plane ($\phi = 0$)

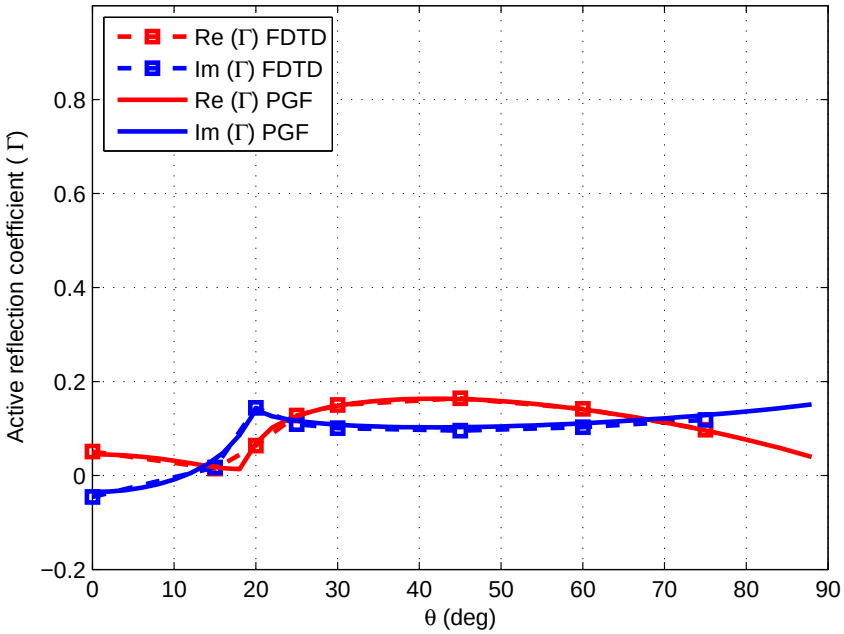

(b) H-plane ($\phi = 90$)

Figure 4.5: Real and imaginary parts of the active reflection coefficient for an infinite array of $\lambda/2$ dipoles with rectangular lattice. The periodicity considered here is $\lambda/2$ and $3\lambda/4$ in the skew and y axes. The characteristic impedance is 50Ω

E- and H- planes are not equal. In order to find the reason of this discordant point, further efforts could be focused on improving the sampling of the reference solution and analyzing the level of convergence. A deep analysis of the behavior of the new code for grating lobes could provide more information about this effect.

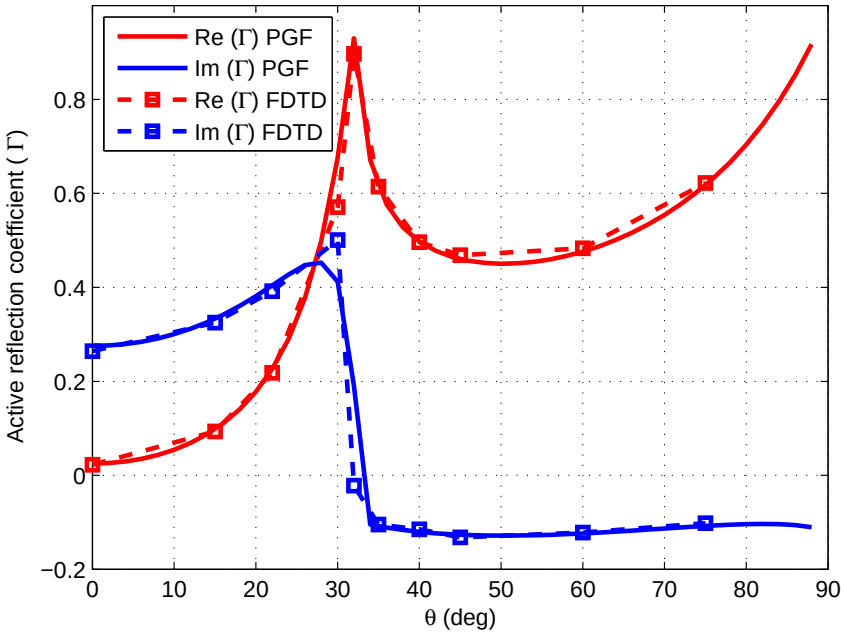

(a) E-plane ($\phi = 0$)

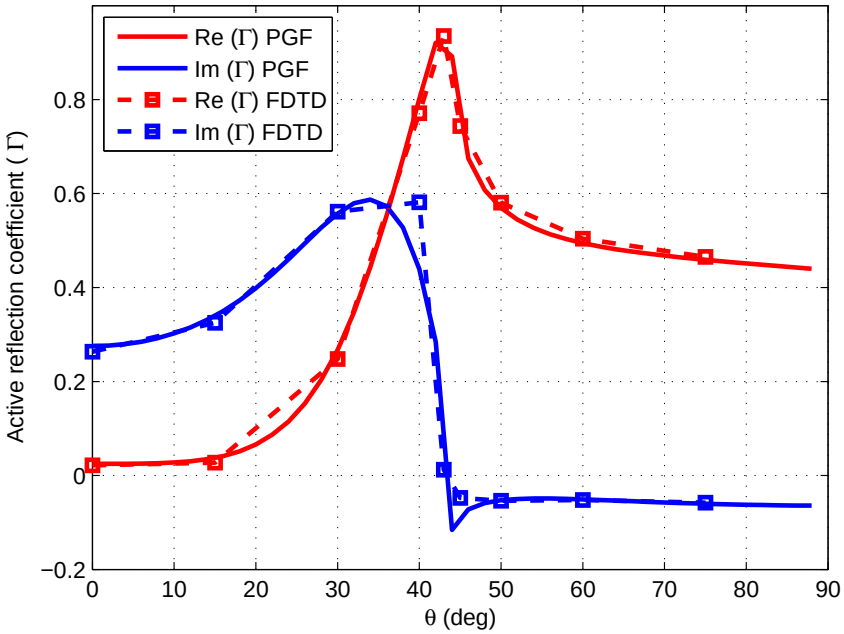

(b) H-plane ($\phi = 90$)

Figure 4.6: Real and imaginary parts of the active reflection coefficient for an infinite array of $\lambda/2$ dipoles with triangular lattice. The periodicity considered here is $3\lambda/4$ in both axes. The characteristic impedance is 50Ω

Chapter 5

Implementation of the ASM-MBF method

The ASM-MBF method is now implemented in the MoM's code modified in chapter 3 for solving 2D finite planar arrays with rectangular and skew lattices. The aim of this new program is to improve the computation time and the memory requirements by reducing the system of equations. The code created for solving 2D infinite arrays, together with the original code, are used to extract the surface current distributions employed as macro basis functions. The structure and the algorithm of the new code are firstly introduced to the reader. The parameter relating the number of macro basis functions used after the SVD procedure is optimized for an straightforward case. Finally, the code is verified against the original MoM's code in terms of accuracy and computation time for 2 types of arrays containing dipoles of $\lambda/2$ and bowties respectively.

5.1 ASM-MBF algorithm

The ASM-MBF method has been implemented in a new function called *ASMsolver.m*. This function has 4 input parameters: N_s and N_y, defining the dimensions of the desired array in both skew and y directions, and D_s and D_y, specifying the separation between antennas in both axes. As shown in figure 5.1, the structure of *ASMsolver.m* consists on 9 different scripts. The ones highlighted in red are new scripts created or modified in this project. The others were already predefined in the original MoM's code.

The algorithm follows the procedure explained in the background theory for the ASM-MBF method. The set of macro basis functions is extracted from 3 scripts: *infiniteMBF.m*, *edgeMBF.m* and *SVDprocedure.m*. The algorithm implemented in each one is explained below:

- *infiniteMBF.m*: The macro basis functions representing the inner currents of the array are extracted with the ASM. First of all, the file containing the mesh of the basic antenna is loaded. The surface current distributions for N^2 different phase-shifts are solved. The program implemented in chapter 4 is used for this purpose. This set of infinite currents are applied to the ASM formula (2.38) so as to solve the N^2 inner current distributions. The extracted currents will be saved in *innerMBF.mat*.

- *edgeMBF.m*: The macro basis functions for the edge array effects are solved here. The script *array_creator.m* is employed for creating a 2×2 array from the analyzed antenna. The full-wave solution of this array is obtained using the brute-force code.

That is, the following sequence of scripts are executed: *rwg1.m*, *rwg2.m*, *rwg3.m* and *rwg4.m*. As the analyzed array has 4 antennas, we will obtain 4 surface current distributions which will be saved in *edgeMBF.mat*.

- *SVDprocedure.m*: The whole set of macro basis functions is orthogonalized applying the SVD procedure. The files containing the macro basis functions are loaded first and joined forming a matrix. The SVD decomposition is then applied to the resulting matrix. We will take as many orthogonal functions as eigenvalues over the threshold. The optimum threshold is analyzed in the next section. The definitive set of MBFs is saved in *reduced_matrix.mat*.

Once the set of macro basis functions is solved, the main part of the algorithm is executed. That is, the construction of the RWG impedance matrix, the excitation vector and the reduction of the equation system with the extracted MBFs. This procedure is included in the following sequence of scripts: *array_creator.m*, *rwg1.m*, *rwg2.m*, *rwg3.m*, *rwg4.m* and *rwg5.m*.

- *array_creator.m*: The array is built from the basic antenna mesh file. The skew angle is specified inside this script.

- *rwg1.m*: This script belongs to the MoM's code and calculates the basic parameters of the discretized array. That is, those parameters related to the triangles and edges.

- *rwg2.m*: This script also belongs to the MoM's code. The vector containing the 9 subtriangle midpoints for every triangle and other parameters of the RWG basis functions are calculated.

- *rwg3.m*: This script keeps the same structure that the original included in the MoM's code. However, we have included one flag. When the flag is 1, the impedance matrix is built like in the original script. When the flag is 0, the periodic Green's function is used instead of the 3D Green's function. The function computing these 2 procedures is called *RWGmatrix.m*. When the flag is 2, the script *rwg3.m* executes *ASMmatrix.m*. This function will be applied in this case. The impedance matrix is built and reduced applying the product in (2.43) with the set of MBFs included in *reduced_matrix.mat*. However, the RWG impedance matrix and the reduced matrix are not constructed by brute-force. The property of Toeplitz-symmetric matrix mentioned in chapter 3 is used here. Only a part of the RWG impedance matrix is built, but not at the same time. Just the mutual coupling between one antenna and the rest of the array is computed and reduced every time. Then, the memory requirements will be improved. Following this procedure, we will obtain one part of the whole reduced matrix. Applying the Toeplitz-symmetric property the entire matrix is constructed.

- *rwg4.m*: This script preserves the structure of the MoM's code, but we have included a flag. When the flag is different of 0, the original code is executed. When the flag is 0, the excitation vector is built and reduced with the equation in (2.44). The resultant reduced system of equations is solved with LU decomposition finding the reduced set of coefficients belonging to the MBFs. The RWG coefficients are solved by performing the weighted sum of the MBFs for every antenna of the array.

- *rwg5.m*: The surface current distribution is calculated from the RWG intensity coefficients. This script belongs to the original MoM's code.

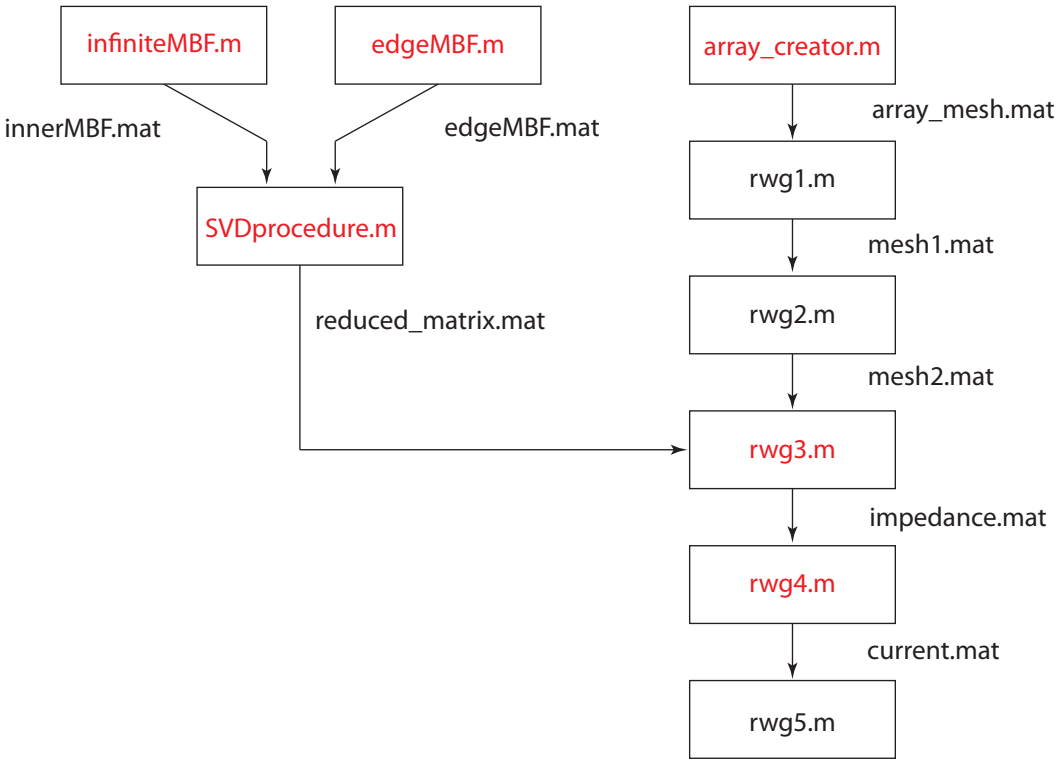

Figure 5.1: Flowchart of *ASMsolver.m*

5.2 Threshold optimization for the SVD procedure

The orthogonalization of the obtained macro basis functions is necessary for avoiding ill-conditioned equation systems. One or more vectors can be linear combination of the set. In this case, when the matrix of MBFs is applied to the equation system, the reduced system can be vulnerable to small variations. That is, a small error can lead to great inaccuracies.

The resultant set of orthogonalized MBFs is defined by the first matrix of the decomposition, $\mathbf{S}$. It is not necessary to consider all the MBFs for achieving a good accuracy. For that reason, the SVD procedure sets a certain threshold for the singular values of the diagonal matrix, $\mathbf{V}$. The number of resultant macro basis functions will be the same that the number of singular values above this threshold. In order to find the optimum threshold, the new program is tested with a simple case. A dipole antenna of $\lambda/2$ working at 75 MHz, 0.02 m of width and 39 non-boundary edges have been chosen for this section. We have already checked other improvements with this type of antenna in previous chapters because of being the most simple and well-studied antenna geometry. In figure 5.2 (a) a set of array of dipoles with dimensions going from 2×2 to 8×8 have been computed for different thresholds. The periodicity is $\lambda/2$ in the skew direction and $3\lambda/4$ in the y direction for rectangular lattice. The the relative error is computed from the maximum error of all the input impedances calculated for a given threshold. The reference value here is the brute-force solution. The number of extracted MBFs here is 8, 4 from the ASM and 4 from the edge array solution. In figure 5.2 (b), it is shown the same situation but extracting 13 MBFs. That is, 9 from the ASM and 4 from the edge array solution. For both cases,

when the threshold is reduced, the number of MBFs increases improving the accuracy of the results. From this results one can conclude that exists a trade-off between the number of MBFs employed and the accuracy. If we choose a non-restrictive threshold, the accuracy will improve but the dimensions of the reduced matrix will grow increasing the time spent solving the reduced system. For the following section, the value of the chosen threshold is 10^{-3} because with just 4 MBFs the relative error remains below $10^{-2}\%$ in both cases, which is negligible in comparison with the error produced by the MoM's code.

5.3 Verification of the ASM-MBF method code

The new code implementing the ASM-MBF method is finally tested in terms of computation time and accuracy. The same array of dipoles has been chosen for this case due to the simplicity of the geometry. In figure 5.3 (a), the computation time spent in the solution of the equation system is analyzed for the brute-force case, that is, the original MoM's code adapted in chapter 3 for rectangular and skew lattices. The time spent involving the extraction of the orthogonalized set of MBFs, the reduction of the RWG system and the solution of the reduced system is also analyzed for the created code. We have considered 3 cases, when 1 (N=1), 4 (N=2) and 9 (N=3) MBFs are obtained from the ASM. The computation time is evaluated in all cases for a range of arrays with dimensions going from 2×2 to 13×13. In figure 5.3 (b), the relative error of the input impedance is evaluated for this 3 cases. It is calculated as the maximum relative error for all the input impedances of each array. The reference value is obtained from the brute-force method. The computation time is almost constant respect to the original MoM's code. This fact is produced because the time spent in the reduction and solution of the system is negligible in front of the extraction of the MBFs. As the computation time with the brute-force grows with $\sim (M \times M)^5$, the computation time, for N=1, improves for arrays equal or larger than 8×8 dimensions with a negligible constant relative error of $10^{-2}\%$. When more MBFs are used, this constant time increases making the new code efficient for arrays of larger dimensions and improving slightly the relative error.

For this analyzed case, only 1 MBF extracted from the ASM and the MBFs obtained from the edge effects are enough for improving the results of the original code in terms of computation time for arrays larger than 8×8 dimensions obtaining the same accuracy. If we are solving arrays of different dimensions with the same type of antenna, the calculation of the MBFs is only necessary the first time. Hence, this offset time can be removed making the new code even more efficient in terms of computation time.

In figure 5.4, the computation time and the relative error have been analyzed for the same case but with skew axes. The skew angle introduced is $\varphi = 30°$. The obtained results agree with the rectangular lattice. When the ASM-MBF method uses 9 MBFs extracted from the ASM (N=3), the relative error of the input impedance increases respect to the rectangular lattice. The number of MBFs employed after the SVD procedure is 4 for both lattices. Thus, this problem probably is produced for the dipole geometry with skew lattice. One possible solution is to change the threshold in order to obtain more MBFs after the SVD procedure.

The improvements of new code in terms of computation time and accuracy have been verified for the most simple case. The next step is testing the program for arrays constituted by more complex antennas. A bowtie antenna made of PEC has been chosen for this case (figure 5.5). The width of the bowtie is $w = \lambda/2$ and the longitude is $l = \lambda/2$. The working frequency is 750 MHz and it has 375 inner edge elements. The periodicity considered here is $3\lambda/4$ for both x and y directions.

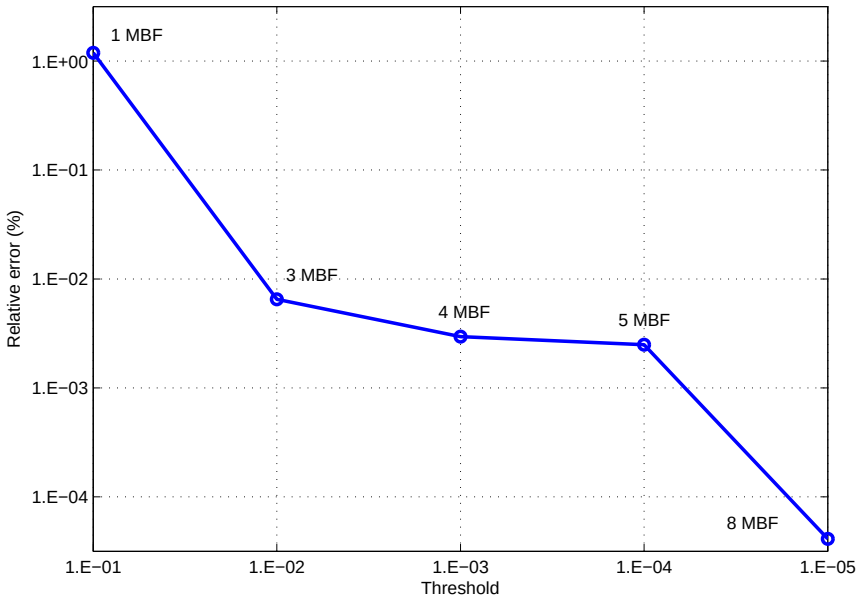

(a) Maximum relative error of the input impedance for 4 + 4 MBFs

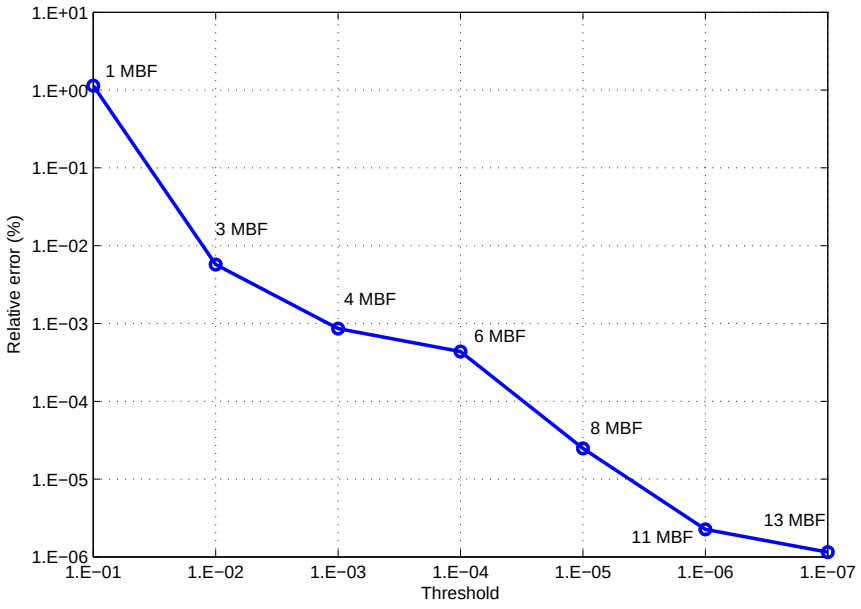

(b) Maximum relative error of the input impedance for 9 + 4 MBFs

Figure 5.2: Evaluation of the maximum relative error of the input impedance for a given threshold. Array of dipoles for rectangular lattice in the broadside direction from 2×2 to 8×8 dimensions

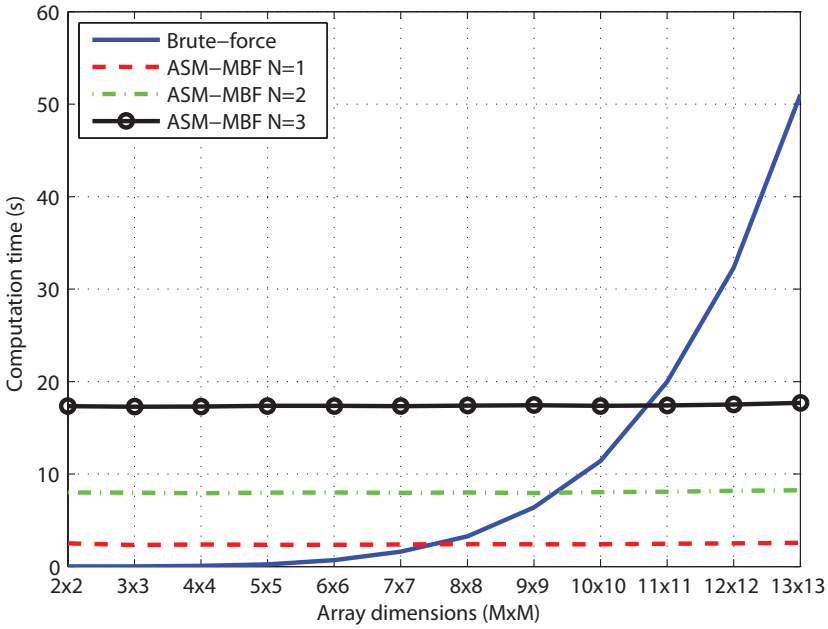

(a) Computation time related to the solution of the equation system. For the ASM-MBF case, it includes the time regarding the extraction of the MBFs, the reduction and the solution of the system of equations

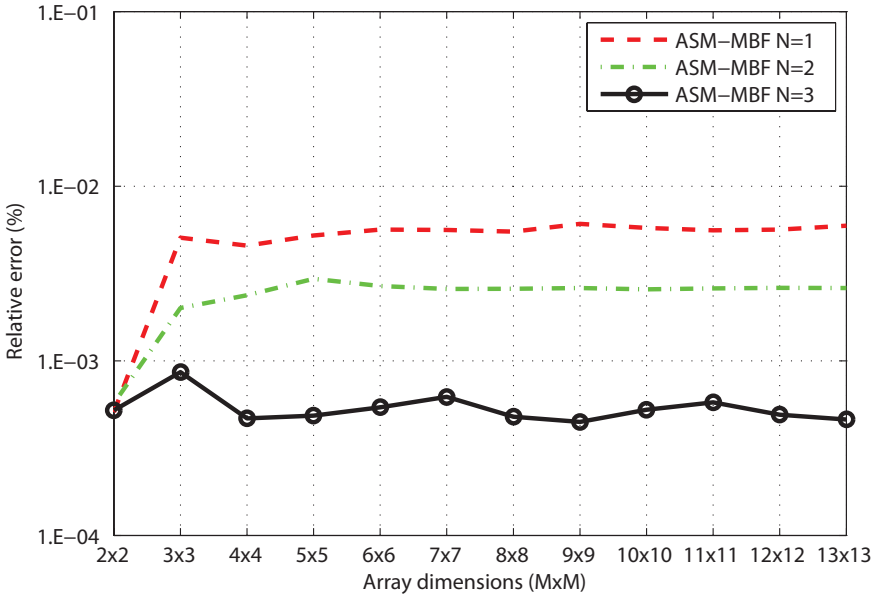

(b) Maximum relative error of the input impedance

Figure 5.3: Array of dipoles for rectangular lattice

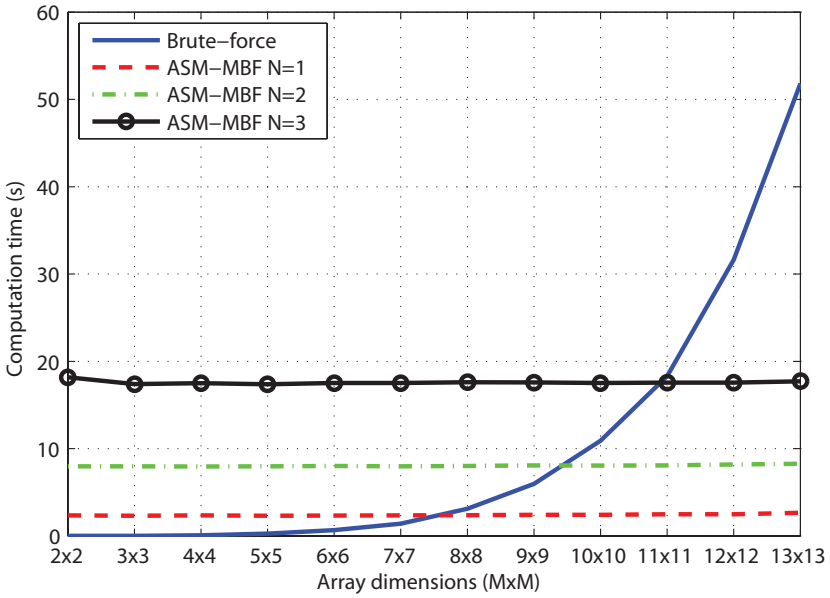

(a) Computation time related to the solution of the equation system. For the ASM-MBF case, it includes the time regarding the extraction of the MBFs, the reduction and the solution of the system of equations

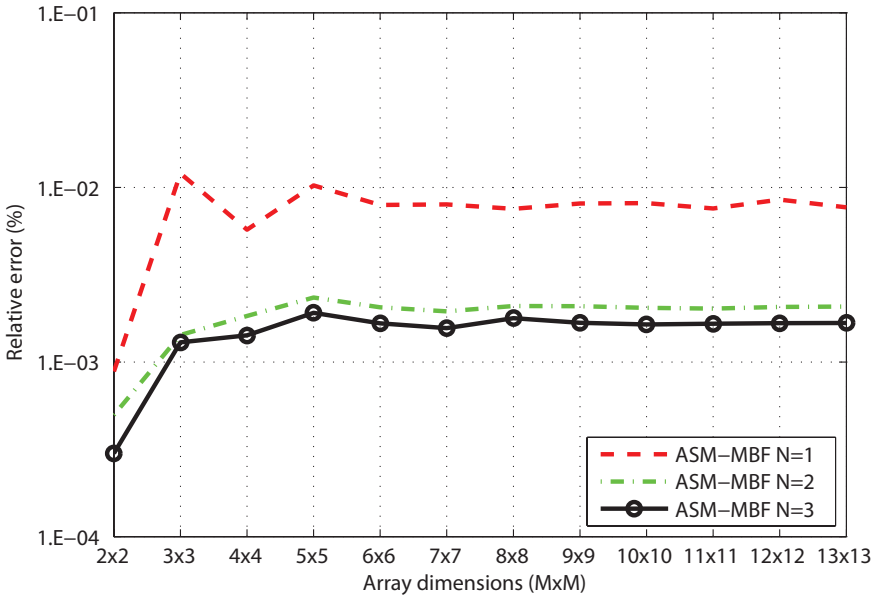

(b) Maximum relative error of the input impedance

Figure 5.4: Array of dipoles for skew lattice with $\varphi = 30°$

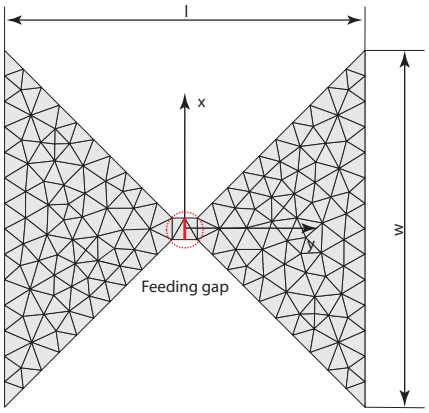

Figure 5.5: Structure of the bowtie antenna analyzed in the example and the mesh used. This mesh consists of 375 non-boundary edges

In figure 5.6, the computation time for solving the equation system and the maximum relative error of the input impedance are analyzed for the case of bowtie arrays with rectangular lattice. The range of arrays analyzed goes from 2×2 to 8×8 dimensions. As shown in figure 5.6 (a) , the arrays larger than 5×5 can not be solved by brute-force due to memory limitations. That is, Matlab is unable to save impedance matrices larger than 9375×9375 in our case, where 9375 is the total number of unknowns for this array. In the ASM-MBF method, the RWG impedance matrix is also built before being reduced. However, the new program calculates and stores the impedance parameters in various steps. Furthermore, the Toeplitz-symmetric property is used in order to avoid building the whole RWG impedance matrix. The efficient usage of the memory performed in the new code enables solving larger arrays.

The time spent with the new code for the 3 cases is almost constant respect to the brute-force case. The offset time produced due to the extraction of the MBFs has increased in this case. The main reason is because the basic meshes now have more edge elements. If we compare this results with the dipole case, one can observe that the curves are not perfectly constant. As the number of edge elements is higher, the time spent in reducing every block of the impedance matrix increases. The time for solving the reduced matrix will be almost the same than in the dipole case because the dimensions of the matrix only depends on the number of antennas contained in the array and the number of MBFs employed.

The relative error is below 1% when using 4 and 9 MBFs from the ASM for the range of arrays analyzed (2×2 to 5×5). This error is insignificant respect to the error produced by the RWG discretization. When 1 inner MBF is used, the relative error reaches a significant value between 5 and 10%. We can not be sure if the error is produced due to the original program or the ASM-MBF method. In the MoM based on RWG functions, when the array dimensions increase, the condition number becomes huge. This means that small variations can lead to big inaccuracies. With the new method all the MBFs are extracted from small and basic antenna meshes. Hence, the condition number of the reduced matrix will be reduced. That is, this implemented method could improve the accuracy of the results for large arrays of complex antennas. Further efforts will be focused on verifying this hypothesis by comparing the results with the brute-force solution of an array with a more refined mesh or with other software employing a different method. The same results have been obtained with this array of bowties, but for skew lattice ($\varphi = 30°$)

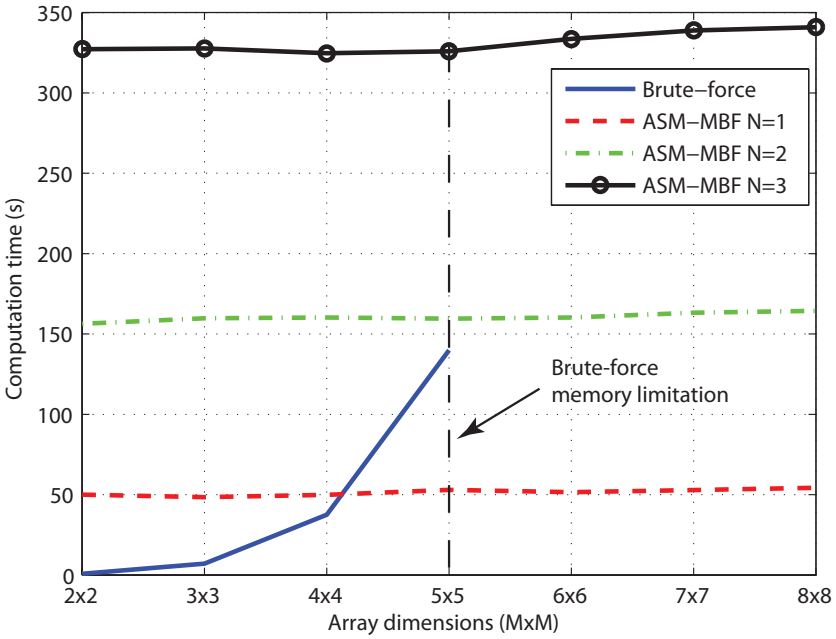

(a) Computation time related to the solution of the equation system. For the ASM-MBF case, it includes the time regarding the extraction of the MBFs, the reduction and the solution of the system of equations

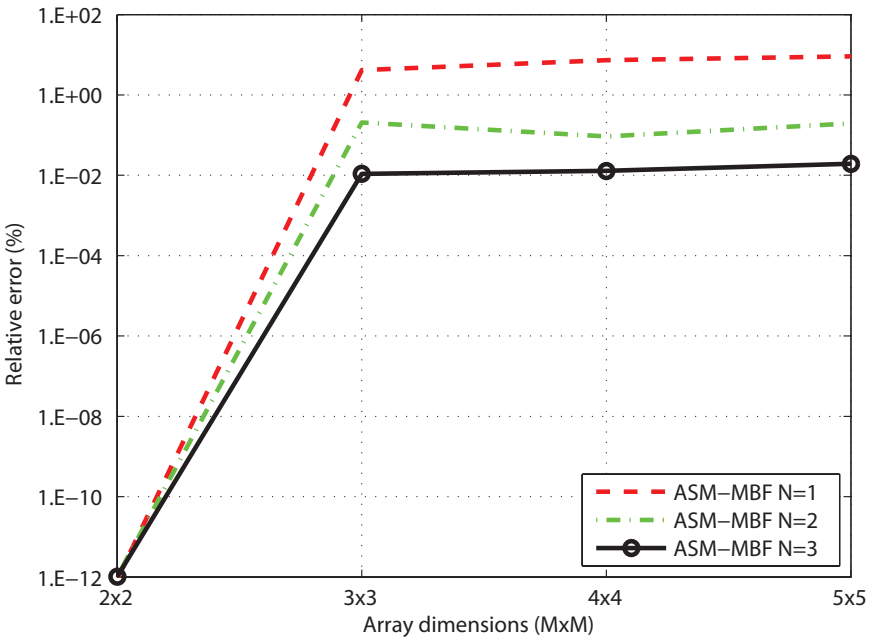

(b) Maximum relative error of the input impedance

Figure 5.6: Array of bowties for rectangular lattice

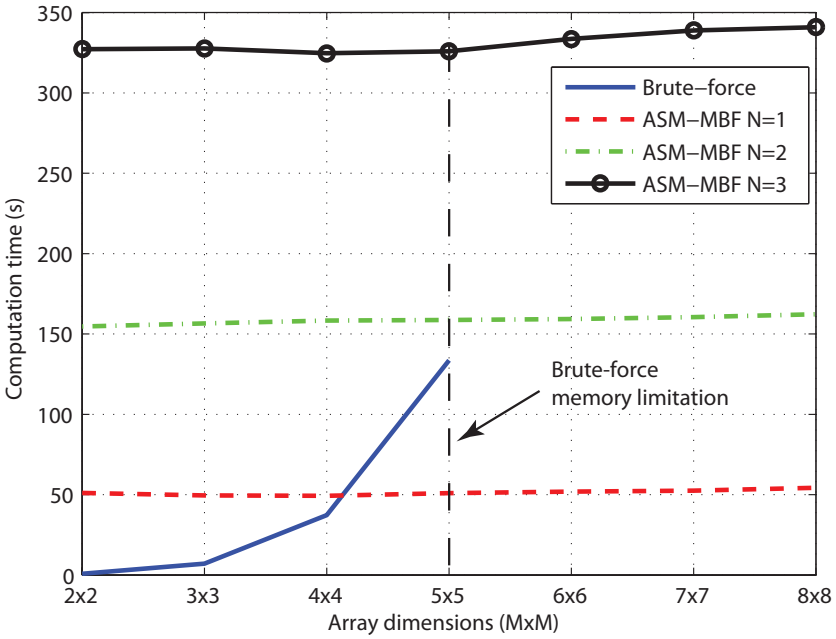

(a) Computation time related to the solution of the equation system. For the ASM-MBF case, it includes the time regarding the extraction of the MBFs, the reduction and the solution of the system of equations

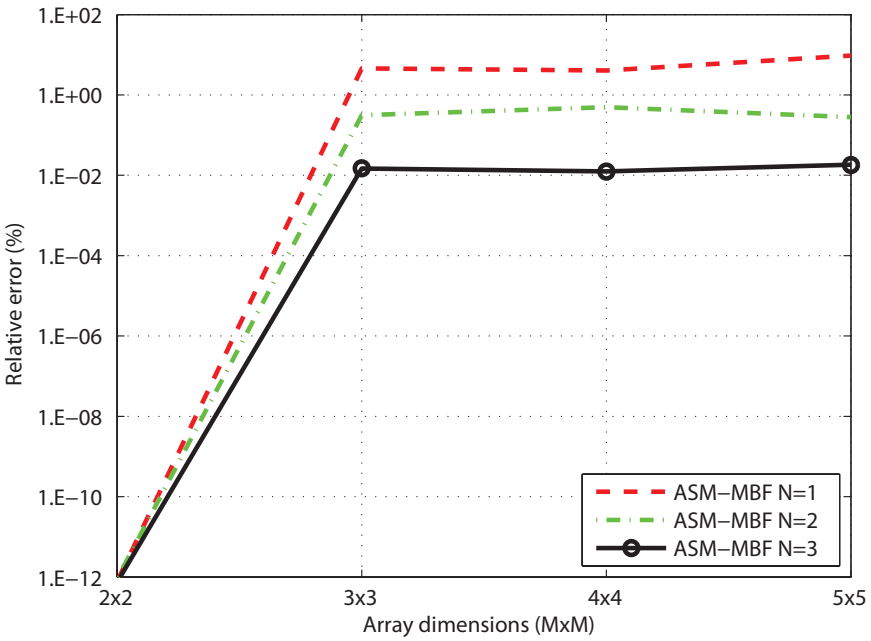

(b) Maximum relative error of the input impedanc

Figure 5.7: Array of bowties for skew lattice with $\varphi = 30°$

Chapter 6

Conclusions and future work

In this report, the existing code implementing the Moment's Method based on the subsectional RWG basis function has been modified for solving, firstly, 2D planar infinite arrays of antennas and, secondly, 2D planar large-scaled finite arrays with the ASM-MBF method. A new script has been implemented and added to the basis program so as to obtain arbitrary 2D array meshes from a single antenna mesh for rectangular and skew lattices. Moreover, the part of the code corresponding to the excitations has also been modified for feeding all the antennas conforming the array. For the feeding points, the modification also allows to introduce a phase-shift for y and skew directions. The construction of the impedance matrix has been optimized in terms of computation time without compromising the accuracy. For instance, for the 2-dimensional array of dipoles analyzed in figures 3.5, 3.6 and 3.7 for different dimensions, the maximum relative error of the input impedance for every antenna port remains constant and below 10^{-4}%. The original code has been evaluated for the case of 2 dipoles in section 3.4 taking as a reference the results from the *4nec2* program. The relative error is around 1%. Hence, the error in the input impedance produced by the matrix optimization is negligible.

The infinite array program has been created replacing the 3D Green's function for the 3D periodic Green's function. The Floquet theorem has been applied to the infinite array case to solve this problem as a single cell with quasi-periodic boundaries. The resultant expression contains the periodic Green's function. The function consists of a very slowly convergent series. The Edwald's method has been justified as the best acceleration technique because only few terms are needed for achieving an excellent accuracy in the region of the antenna cell, and independently of the z coordinate. The time spend for computing every term with this method is longer than in the other cases analyzed due to the erfc function. However, it has proven as the fastest one, especially for high accuracies. The new program has finally been tested for an infinite array of dipoles with rectangular and skew axes taking as a reference the results obtained from PBFDTD software based on FDTD theory. The active reflection coefficient for the antenna cell analyzed for different scanning angles matches perfectly, even in presence of grating lobes, except for punctual points.

Finally, the ASM-MBF method has been implemented over the original MoM's code. The infinite array code has been utilized for extracting the currents used for calculating the MBFs with the ASM representing the inner currents. The original program has been used for the MBFs expressing the edge current effects. The whole set of functions has been orthogonalized with the SVD procedure in order to avoid inaccuracies produced by an ill-conditioned equation system. The effect of the threshold defined in this procedure has been checked in figure 5.1. The results show a trade-off between the maximum error of the input

impedance of the antenna port and the number of MBFs used. This means that if a high accuracy is required, the threshold will be less restrictive and the number of functions used will be larger, increasing the dimensions of the reduced system and the computation time. The efficiency of the program has been verified in terms of computation time and relative error using a different number of MBFs for arrays of dipoles and bowties. For the first type of arrays, the computation time is improved for arrays larger than 8×8 antennas for both rectangular and skew lattices when just 5 MBFs are calculated. The maximum relative error of the input impedance ports respect to the MoM's program is negligible in this case. For the bowties arrays, the relative error is between 5% and 10% using the minimum number of MBFs. Here, the computation time is also improved for arrays larger than 5×5. The condition number can be the cause of this notable error. That is, the huge condition number of the original impedance matrix used for the reference solutions can produced inaccuracies. It should be remarked that the time spend with the new method is generally due to the calculation of the MBFs with ASM and hence almost independently of the array dimensions for the analyzed cases.

Future efforts will be focused on the following goals:

- Tabulating the 3D periodic Green's function for reducing the computation time of the MBFs extracted with the ASM.
- Expanding the method for PEC antennas with finite ground plane.
- Including the necessary formulation for analyzing dielectric materials.
- Analyzing the condition number of the impedance matrix for the MoM's code and the new program in order to find out the origin of the noticeable errors obtained for bowtie arrays.
- Verifying whether the ASM-MBF method reduces the condition number due to the use of MBFs extracted from simple meshes.
- Comparing the results obtained with the ASM-MBF method with the MoM's code using a more refined mesh or with a commercial software based on other method.

Bibliography

[1] C. A. Balanis, *Advanced Engineering Electromagnetics*. John Wiley and Sons, 1989.

[2] C. A. Balanis, *Antenna Theory: Analysis and Design*. 2nd ed. Wiley, New York, 1997.

[3] e. R. C. Johnson, *Antenna Engineering Handbook*. 3rd ed. McGraw-Hill, New York, 1993.

[4] W. C. Gibson, *The method of moments in electromagnetics*. Chapman& Hall/CRC, 2008.

[5] S. Rao, D. Wilton, and A. Glisson, "Electromagnetic scattering by surfaces of arbitrary shape," *Antennas and Propagation, IEEE Transactions on*, vol. 30, pp. 409 – 418, may 1982.

[6] A. Skrivervik and J. Mosig, "Analysis of finite phase arrays of microstrip patches," *Antennas and Propagation, IEEE Transactions on*, vol. 41, pp. 1105 –1114, aug 1993.

[7] A. Neto, S. Maci, G. Vecchi, and M. Sabbadini, "A truncated floquet wave diffraction method for the full-wave analysis of large phased arrays .II. Generalization to 3-D cases," *Antennas and Propagation, IEEE Transactions on*, vol. 48, pp. 601 –611, apr 2000.

[8] C. Craeye and X. Dardenne, "Element pattern analysis of wide-band arrays with the help of a finite-by-infinite array approach," *Antennas and Propagation, IEEE Transactions on*, vol. 54, pp. 519 –526, feb. 2006.

[9] R. Maaskant, R. Mittra, and A. Tijhuis, "Fast analysis of large antenna arrays using the characteristic basis function method and the adaptive cross approximation algorithm," *Antennas and Propagation, IEEE Transactions on*, vol. 56, pp. 3440 –3451, nov. 2008.

[10] V. P. J. Yeo and R. Mittra, "Efficient analysis of a class of microstrip antennas using the characteristic basis function method (CBFM)," *Microwave Opt Technol Lett 39*, pp. 456 –464, 2003.

[11] R. S. C. Craeye, "Finite array analysis through combination of macro basis functions and array scanning methods," *ACES journal on*, vol. 23, no. 3, 2008.

[12] S. N. Makarov, *Antenna and EM Modeling with MATLAB*. Wiley-interscience, 2002.

[13] X. Dardenne and C. Craeye, "Method of moments simulation of infinitely periodic structures combining metal with connected dielectric objects," *Antennas and Propagation, IEEE Transactions on*, vol. 56, pp. 2372 –2380, aug. 2008.

[14] N. Guerin, C. Craeye, and X. Dardenne, "Accelerated computation of the free space Green's function gradient of infinite phased arrays of dipoles," *Antennas and Propagation, IEEE Transactions on*, vol. 57, pp. 3430 –3434, oct. 2009.

[15] R. J. Mailloux, *Phased Array Antenna Handbook*. Artech house, inc., 1993.

[16] G. Valerio, P. Baccarelli, P. Burghignoli, and A. Galli, "Comparative analysis of acceleration techniques for 2-D and 3-D Green's functions in periodic structures along one and two directions," *Antennas and Propagation, IEEE Transactions on*, vol. 55, pp. 1630 –1643, june 2007.

[17] K. E. Jordan, G. R. Richter, and P. Sheng, "An efficient numerical evaluation of the Green's function for the Helmholtz operator on periodic structures," *Journal of Computational Physics*, vol. 63, no. 1, pp. 222 – 235, 1986.

[18] A. M. G. M. G. Tiberi, M. Degiorgi and R. Mittra, "A class of physical optics-SVD derived basis functions for solving electromagnetic scattering problems," *presented at the Antennas and Propagation Society Int. Symp., Washington, DC*, pp. 3 –8, july 2005.

[19] MathWorks, "How does the backslash operator work when A is full." `http://mathworks.com/support/solutions/en/data/1-172BD/index.html?product=ML&solution=1-172BD`, june 2009.

[20] C. Leat, N. Shuley, and G. Stickley, "Triangular-patch model of bowtie antennas: validation against Brown and Woodward," *Microwaves, Antennas and Propagation, IEE Proceedings* -, vol. 145, pp. 465 –470, dec 1998.

[21] V. Arie, "NEC based antenna modeler and optimizer." `http://home.ict.nl/~arivoors/`, march 2011.

[22] G. J. Burke and A. J. Poggio, "Numerical electromagnetics code (NEC) -Method of moments," *Rep. UCID18834, Lawrence Livermore Lab., CA*, jan 1981.

[23] W. Andre, "Computation of the comple error function." `http://dip.sun.ac.za/~weideman/research/cef.html`, december 1997.

[24] F. Capolino, D. Wilton, and W. Johnson, "Efficient computation of the 3D Green's function with one dimensional periodicity using the Ewald method," in *Antennas and Propagation Society International Symposium 2006, IEEE*, pp. 2847 –2850, july 2006.

[25] "Periodic Boundary FDTD (PBFDTD) Program, written by Henrik holter. Stockholm, Sweden,"

[26] H. Holter and H. Steyskal, "Some experiences from FDTD analysis of infinite and finite multi-octave phased arrays," *Antennas and Propagation, IEEE Transactions on*, vol. 50, pp. 1725 – 1731, dec 2002.